Sterile Neutrino Searches

Luis A. Delgadillo

Dissertation submitted to the Faculty of the
Virginia Polytechnic Institute and State University
in partial fulfillment of the requirements for the degree of

Master of Science
in
Physics

Patrick Huber, Chair
Thomas O'Donnell
Shunsaku Horiuchi
Ian Shoemaker

May 10, 2021
Blacksburg, Virginia

Keywords: Neutrino oscillations, Sterile neutrinos

Sterile Neutrino Searches

Luis A. Delgadillo

Abstract

In the first part of the thesis we explore the sensitivity to sterile neutrinos by using a novel kaon tagging technology: ENUBET, the proposed experiment could decisively test indications from the experiments Neutrino-4 and IceCube. In the second part of the thesis we discuss the current status of sterile neutrino searches at nuclear reactors, we present a study with the optimization of a green field, two baseline reactor experiment with respect to the sensitivity for electron anti-neutrino disappearance in search of a light sterile neutrino at both *research* and *commercial* reactors. We find that a total of 5 tons of detectors deployed at a commercial reactor with a closest approach of 25 m can probe the mixing angle $\sin^2 2\theta$ down to $\sim 5 \times 10^{-3}$ around $\Delta m^2 \sim 1\,\mathrm{eV}^2$. The same detector mass deployed at a research reactor can be sensitive up to $\Delta m^2 \sim 20 - 30\,\mathrm{eV}^2$ assuming a closest approach of 3 m and excellent energy resolution, such as that projected for TAO. We also find that lithium doping of the reactor could be effective in increasing the sensitivity for higher Δm^2 values.

Sterile Neutrino Searches

Luis A. Delgadillo

General Audience Abstract

A sterile neutrino is a particle that is not included in the actual content of matter at the fundamental level. Our goal in this thesis was to search for an imprint of this particle at neutrino experiments. We performed numerical simulations using the experimental specification given in the literature to predict what this signal should look like. The importance of searching for this particle arises from indications at neutrino nuclear experiments, if this particle exists, that would imply new physics beyond our actual understanding of the matter content in the universe. The first search was performed at an experimental facility called ENUBET and the second search was performed at nuclear reactors. Testing this elusive particle means we need to determine two parameters from a model. The results of the aforementioned parameter space searches are presented in this thesis. The statistical significance in our findings is not entirely conclusive to either confirm or refute the sterile neutrino. The benefits of studying neutrinos at nuclear reactors is that they are produced in generating electrical power as well as monitoring nuclear weapons.

Acknowledgements

To my advisor, Prof. Dr. Patrick Huber; my committee: Prof. Dr. Thomas O´Donnell, Prof. Dr. Shunsaku Horiuchi and Prof. Dr. Ian Shoemaker. To my family, particularly my brother José Emmanuel Delgadillo. To my friends: Joe Camilleri, Anri Karanovic, Tommy Lam, Ho Lun Tang, Karla Telléz Girón and Arian Vizvaee. To my undergraduate advisor, Prof. Dr. Alfredo Aranda from University of Colima. To my collaborator Dr. Jeffrey Berryman and to the Department of Physics at Virginia Tech.

Contents

List of Figures

List of Tables

1 Introduction

Neutrino physics is a very active and exciting field of research, their increasing connections over the past few years with areas like astrophysics and cosmology have made this field an interdisciplinary science, not only from the experimental point of view but also the theoretical and phenomenological perspectives. Such developments have helped to understand the role that neutrinos play in our understanding of fundamental physics.

In this thesis we will give a brief introduction into the topic of neutrino physics and their historical development as well as their impact in modern day research. We will explain the mechanism of neutrino oscillation in vacuum and matter, their phenomenological consequences and the actual state of the art of neutrino parameters in Sec. 2. Then in Sec. 3 we start talking about the standard model of particle physics and the main features of this theory (without going too deep in the theoretical foundations of the model), the role of neutrino oscillations as proof of physics beyond this model and the phenomenological motivations and consequences of including a sterile neutrino to explain anomalous results from several neutrino experiments. Later in Sec. 4 we discuss our results about sterile neutrino searches at ENUBET, a proposal of an experiment that uses a novel kaon beam technique to reduce systematic errors in the neutrino cross sections. There, we explore the sensitivity to sterile neutrinos from this setup and found decisive ways to test recent indications by two different neutrino experiments. Furthermore in Sec. 5 we review the physics of reactor neutrinos, their impact on determining the status of the three neutrino oscillation framework and outline the so called reactor anti-neutrino anomaly which motivates the present searches of sterile neutrinos at nuclear reactors. Moreover in Sec. 6 we present our results of the optimization of a green field, two baseline neutrino experiment at both *research* and *commercial* nuclear reactors in search of a light sterile neutrino. Last but not least in Sec. 7 we conclude our analysis on sterile neutrino searches and their impact on present and future neutrino physics research.

The history of neutrinos as an experimental discipline starts with the investigation of beta decay, following the determination of discrete lines in the energy spectrum of gamma and alpha rays, it was shocking for James Chadwick [13] to find that the emission of the energy spectrum of beta decay was a continuum. After this observation two main explanations arose: the first one assumed that energy conservation was only statistically valid for those kind of processes and the second explanation was that there was a particle that carries away such energy (W. Pauli). The elusive particle of spin $\frac{1}{2}$ had to be released together with the electron but somehow escaped from detection. This way the energy can be exchanged among the electron and the mysterious particle, explaining the continuous spectrum. Afterwards, this particle was called *neutrino* by Enrico Fermi. The earliest experimental evidence for neutrinos was spotted in the electron capture of ^{37}Ar in a nuclear recoil experiment leaded by G.W. Rodeback and J.S. Allen [14]

$$^{37}\mathrm{Ar} + e^- \rightarrow \ ^{37}\mathrm{Cl} + \nu_e + Q, \tag{1}$$

with a Q value of 816 keV, the measured value was in agreement with theoretical calculations supporting the idea of the neutrino. Neutrinos were not seen until 1956 by Frederick Reines and Clyde Cowan [15], the experiment is based on the inverse beta decay in which an anti-neutrino interact with a proton to generate a positron and a neutron

$$\bar{\nu}_e + p \rightarrow n + e^+. \tag{2}$$

The birth of elementary particle physics starts with the discovery of the electron by J.J. Thomson [16], after this outstanding result, the scientific community started to wonder which other particles could be inside the atom. After the discovery of the electron and nuclei, several other particles were discovered partly due to improvements on particle accelerators and availability to reach higher and higher energies. Several theoretical models predicted the existence of new particles, those discoveries lead to the development of what it is known at present day as the standard model of particle physics. A theory that explains the interaction of elementary particles with the electromagnetic, weak and strong forces.

1.1 The weak interaction

The weak[1] interaction was first discovered and developed in the context of the β-decay of nuclei. Fundamentally through a decay of neutron n in the nucleus into a proton p, electron

[1]Since the mean lives times of decays mediated by it are very long.

e^- and an electron anti-neutrino $\bar{\nu}_e$, respectively

$$n \to p + e^- + \bar{\nu}_e. \tag{3}$$

The central figure that contributed to the development of the theory of weak interactions was Enrico Fermi, by first explaining the phenomena of beta decay. His theoretical approach to the β-decay process [17] closely resembles that of photon γ emission from radioactive nuclei; Fermi's idea was to replace the electromagnetic current J^μ_γ by a combination of a weak lepton current $J^\mu_\ell = \bar{\psi}_e \gamma^\mu \psi_\nu$ and the weak nucleon current $J^q_\mu = \bar{\psi}_n \gamma_\mu \psi_p$ in a Hamiltonian given by

$$H \propto G_F \int d^3x J^\mu_\ell J^q_\mu, \tag{4}$$

were G_F is the so called Fermi constant and γ^μ are the Dirac gamma matrices. This theoretical framework described the low energy weak processes but was not able to fully explain the weak interactions at higher energies. Some time later, it was realized that such processes had a vector and axial structure. For instance, the introduction of a weak current with this type of structure was proposed by Feynman and Gell-Mann [18]

$$J_\mu = \bar{\psi}_e \gamma_\mu (1 - \gamma_5) \psi_\nu + \bar{\psi}_n \gamma_\mu (1 - \gamma_5) \psi_p, \tag{5}$$

where a term in the current $\propto \bar{\psi}\gamma_\mu\psi$ transforms as a vector and the term $\propto \bar{\psi}\gamma_\mu\gamma_5\psi$ transforms as an axial vector under Lorentz transformations.

The development of the modern version of the electroweak theory by Glashow-Weinberg-Salam (GWS) [19, 20, 21] predicted the existence of a neutral boson Z^0 that mediates the so called neutral current processes and the $W^\pm$ charged bosons responsible of the weak charged current interactions. These bosons were further discovered at CERN in 1983 [22, 23], mainly via the channels

$$\begin{aligned} &\bar{u} + u \to Z^0 \to e^+ + e^- \ (\mu^+ + \mu^-) \\ &\bar{d} + d \to Z^0 \to e^+ + e^- \ (\mu^+ + \mu^-) \\ &\bar{u} + d \to W^- \to e^- + \bar{\nu}_e \ (\mu^- + \bar{\nu}_\mu) \\ &\bar{d} + u \to W^+ \to e^+ + \nu_e \ (\mu^+ + \nu_\mu). \end{aligned} \tag{6}$$

The predictions of those vector bosons postulated by the electroweak theory of (GWS) and their further confirmation at CERN established a solid basis of the standard model of particle physics.

1.2 Parity violation in weak interactions

The possibility of parity violation in the weak interactions was pointed out by Lee and Yang [24], before that, the community had considered that all physical processes were invariant under space inversions and thus parity was a good quantum number for all interactions. The *parity* transformation is defined as the inversion in the coordinates in the sense that for a wave function $\psi(x,t)$, under parity transformation: $\mathcal{P}\psi(x,t) \to \psi(-x,t)$, *i.e.* physical processes should not change in a mirror symmetry. A contradiction to this principle in the weak interaction was found in the experiment conducted by Chien-Shiung Wu *et al.* [25] where atoms of ^{60}Co with a known polarization were employed to observe the angular distribution emission of electrons, expecting a transformation: $\mathcal{P}\psi(\theta,t) \to \psi(-\theta,t)$ in a decay given by

$$^{60}\text{Co} \to \ ^{60}\text{Ni}^* + e^- + \bar{\nu}_e. \tag{7}$$

The experiment showed that electrons were emitted backwards to the spin direction of the parent nucleus by first aligning the spin of ^{60}Co in a particular direction perpendicular to a fixed plane of reference and then setting a mirror oriented in parallel to the original plane. Then, when an electron is produced in a direction, forming an angle θ relative to the spin of ^{60}Co, the electron in the mirror image was surprisingly observed to be in a relative angle $\pi - \theta$. This experiment was the first evidence of parity violation in the weak interaction.

1.3 Experimental evidence of muon and tau neutrinos

In 1962 an experiment lead by L. Lederman, M. Schwartz and J. Steinberger [26] discovered the existence of the muon neutrino ν_μ. For instance, if a ν_e and a ν_μ were identical particles then, the conversion $\nu_e + n \to e^- + p$ should occur with the same probability as $\nu_\mu + n \to \mu^- + p$ which is not the case since the former reaction can further produce a ν_e and a $\bar{\nu}_e$ via the muon decay. In a nutshell, the experiment consisted of a primary proton beam reached $\sim \mathcal{O}(10)$ GeV in energy, a fast magnet directed the protons into a beryllium target were the secondary particles arising from such interactions, pions (π), were sent towards the detector and further absorbed in an iron shielding layer decaying via the two-body processes $\pi^+ \to \mu^+ + \nu_\mu$ and $\pi^- \to \mu^- + \bar{\nu}_\mu$ respectively, producing a particular neutrino flux. Moreover, since no electron candidates were observed at the detector, the parent neutrino should be related to the pion decaying into muon and therefore this neutrino correspond to a different species, the muon neutrino ν_μ. It was not until earlier this century that the tau neutrino was discovered by the DONUT collaboration [27] at the Fermi National Accelerator Laboratory (Fermilab) in

2001, via the leptonic decay of the meson: $D_s \to \tau^- + \bar{\nu}_\tau$ as well as the tau decay to electron: $\tau^- \to \nu_\tau + e^- + \bar{\nu}_e$, confirming the three generation structure of leptons in the Standard Model.

2 Neutrino oscillations

The idea the neutrinos can oscillate was first pointed out by Bruno Pontecorvo in 1957 [28], suggesting transitions among neutrinos and anti-neutrinos in a similar fashion to what happens between the $(K^0, \bar{K}^0)$ mesons. Neutrino oscillation between different flavors was proposed in 1962 by Z. Maki, M. Nakagawa and S. Sakata [29]. Whereas the idea of neutrino oscillations was supported by the deficit of solar neutrinos, the so-called solar neutrino problem, that was not the case for experiments in nuclear reactors.

Back in mid 90s the LSND experiment at Los Alamos found a positive signal of neutrino oscillations generated at accelerators traveling a short distance. [2] It was in 1998 when the Super-Kamiokande experiment presented significant evidence of neutrino oscillations produced in the atmosphere [30]. A few years later in 2001, the SNO experiment solved the solar neutrino problem by demonstrating neutrino oscillations arising from the Sun and the conversion to a different flavor when they arrive at Earth [31].

2.1 Neutrino Oscillation in Vacuum

Neutrino oscillations imply that if a neutrino of definite flavor, namely ν_e with definite energy E_ν is produced via weak processes, at a considerable distance L of the source, the probability of finding the initial neutrino in a different flavor state ν_μ is non-zero.

If we consider a neutrino of initial flavor ν_ℓ,[3] these are the states that are detected and participate on the weak interaction. However, the states that propagate and change between them are the mass eigenstates ν_α each with a different mass m_α, with α =(1,2,3) the relation between states is given by:

$$|\nu_\ell\rangle = \sum_\alpha U_{\ell\alpha} |\nu_\alpha\rangle \tag{8}$$

The oscillation probability *i.e.* the probability of having either a neutrino change or remain as an specific flavor state follows from the ultra-relativistic approach and quantum mechanics. Since the momentum of the neutrino is much grater than the mass, a Taylor expansion relates the energy of the neutrino as

$$E_\alpha = \sqrt{p^2 + m_\alpha^2} \simeq p + \frac{m_\alpha^2}{2p} \simeq p + \frac{m_\alpha^2}{2E_\alpha}, \tag{9}$$

[2] We will talk about this experiment more in depth in the next sections.

[3] ℓ = (e,μ,τ)

the evolution of states in vacuum starting in the mass basis is described by $H_0 \left|\nu_\alpha\right\rangle = E_\alpha \left|\nu_\alpha\right\rangle$, satisfying the time dependent Schrödinger equation:

$$i\frac{\partial}{\partial t}\left|\nu_\alpha(t)\right\rangle = H_0 \left|\nu_\alpha(t)\right\rangle . \tag{10}$$

Therefore, time dependent states are related to the time independent states by a unitary time evolution operator $\left|\nu_\alpha(t)\right\rangle = e^{-iE_\alpha t}\left|\nu_\alpha\right\rangle$, where the Hamiltonian in the flavor basis is related by a similarity transformation $H_f = R(\theta)H_0R^T(\theta)$ to the original mass basis, being $R(\theta)$ an orthogonal matrix.

On the other hand, the evolution of the flavor eigenstates is given by the relation:

$$\left|\nu_\ell(t)\right\rangle = \sum_\alpha e^{-iE_\alpha t}U_{\ell\alpha}\left|\nu_\alpha\right\rangle , \tag{11}$$

were the unitary matrix $U_{\ell\alpha}$ is regularly named as the Pontecorvo-Maki-Nakawaga-Sakata (PMNS) [28, 29]. For the case of n flavors with n different mass eigenstates, the most general form of the $n \times n$ unitary mixing matrix $U_{\ell\alpha} = U_{\mathsf{PMNS}}$ can be parameterized by means of $n(n-1)/2$ mixing angles and $n(n+1)/2$ corresponding phases. Furthermore, if neutrinos ν_α are of Dirac nature; out of the $n(n+1)/2$ phases, only $(n-1)(n-2)/2$ are physical and will contribute to the conjugation of charge and parity (CP) violation of leptons. Nevertheless, if neutrinos are of Majorana type,[4] the mixing matrix has $(n-1)$ additional physical phases [32].

The probability that a neutrino of a particular flavor change into another is given by

$$P_{\nu_\ell\to\nu_{\ell'}} = \left|\left\langle\nu_{\ell'}|\nu_\ell(t)\right\rangle\right|^2, \tag{12}$$

where

$$\left\langle\nu_{\ell'}|\nu_\ell(t)\right\rangle = \sum_{\alpha,\beta}\left\langle\nu_\beta\right| U^\dagger_{\beta\ell'}e^{-iE_\alpha t}U_{\ell\alpha}\left|\nu_\alpha\right\rangle . \tag{13}$$

For instance, the probability of transition between electron neutrino to muon neutrinos considering the effective two flavor approximation is:

$$P_{\nu_e\to\nu_\mu} = \left|\left\langle\nu_\mu|\nu_e(t)\right\rangle\right|^2 = \sin^2 2\theta_{12}\sin^2\left(\frac{\Delta m^2_{21}L}{4E}\right). \tag{14}$$

[4]In our searches for sterile neutrinos at ENUBET and nuclear reactors, we will consider that neutrinos are of Dirac nature.

2.1.1 2-flavor neutrino oscillations

The simplest model of neutrino oscillations consider the transitions between two neutrino mass eigenstates $|\nu_1\rangle$ and $|\nu_2\rangle$, with definite masses m_1 and m_2; for instance: an electron neutrino at time $t = 0$ is given by the combination

$$|\nu_e\rangle = \cos\theta\,|\nu_1\rangle + \sin\theta\,|\nu_2\rangle\,, \tag{15}$$

and similarly for the muon neutrino

$$|\nu_\mu\rangle = -\sin\theta\,|\nu_1\rangle + \cos\theta\,|\nu_2\rangle\,. \tag{16}$$

Where the angle θ measures the degree of mixing between the mass states, usually referred as the mixing angle. The evolution in time of the muon neutrino state is represented as

$$|\nu_\mu(t)\rangle = -e^{-iE_1 t}\sin\theta\,|\nu_1\rangle + e^{-iE_2 t}\cos\theta\,|\nu_2\rangle\,, \tag{17}$$

where E_1 and E_2 are the corresponding energies associated to the mass states, and we use natural units, where $\hbar = c = 1$. For ultra relativistic neutrinos $E_\nu \gg m_\nu$ therefore

$$\begin{aligned} |\nu_\mu(t)\rangle &= -e^{-it(p+\frac{m_1^2}{2E_\nu})}\sin\theta\,|\nu_1\rangle + e^{-it(p+\frac{m_2^2}{2E_\nu})}\cos\theta\,|\nu_2\rangle\,, \\ |\nu_\mu(t)\rangle &= e^{-it(p+\frac{m_1^2}{2E_\nu})}\Big[-\sin\theta\,|\nu_1\rangle + e^{i\frac{\Delta m^2}{2E_\nu}t}\cos\theta\,|\nu_2\rangle\Big], \end{aligned} \tag{18}$$

where we define the mass splitting $\Delta m^2 = m_1^2 - m_2^2$ and since neutrinos propagate closest to the speed of light, we can approximate $t \sim L$; with L being the distance to the source of muon neutrinos. Such that the probability $P_{\nu_\mu\to\nu_e}$ of transitions between the muon neutrino to electron neutrino after some distance traveled L, is computed by means of the amplitude square $\big|\,\langle\nu_e|\nu_\mu(t)\rangle\,\big|^2$, and since the neutrino eigenstates satisfy the orthonormality condition $\langle\nu_i|\nu_j\rangle = \delta_{ij}$

$$P_{\nu_\mu\to\nu_e} = \big|\,\langle\nu_e|\nu_\mu(t)\rangle\,\big|^2 = \big|\cos\theta\sin\theta(1 - e^{i\frac{\Delta m^2}{2E_\nu}t})\big|^2, \tag{19}$$

and invoking the trigonometric identity: $\sin 2\theta = 2\cos\theta\sin\theta$, we can further simplify to

$$P_{\nu_\mu\to\nu_e} = \sin^2 2\theta\sin^2\Big(\frac{\Delta m^2 L}{4E_\nu}\Big). \tag{20}$$

In units where the baseline $[L] = \mathrm{m}$, the mass splitting $[\Delta m^2] = \mathrm{eV}^2$ and the neutrino energy $[E_\nu] = \mathrm{MeV}$, there is a factor of 1.27 that gives the conversion into these particular units,

which is a commonly used formula for the 2-flavor neutrino oscillations at relatively low energies and baselines

$$P_{\nu_\mu \to \nu_e} = \sin^2 2\theta \sin^2 \Big(\frac{1.27 \Delta m^2 L}{E_\nu}\Big). \tag{21}$$

The mixing angle $\sin^2 2\theta$ determine the amplitude of the oscillation, whereas Δm^2 is involved in the oscillation frequency pattern, the ratio L/E_ν is crucial in resolving the sensitivity scope for Δm^2. Furthermore, since the probability for neutrino oscillations must satisfy the condition: $P_{\nu_\mu \to \nu_e} + P_{\nu_\mu \to \nu_\mu} = 1$. Therefore, the probability that a muon neutrino remain in the same flavor state after some distance traveled L is given by

$$P_{\nu_\mu \to \nu_\mu} = 1 - \sin^2 2\theta \sin^2 \Big(\frac{1.27 \Delta m^2 L}{E_\nu}\Big). \tag{22}$$

In the next sections, we will discuss this model in more detail but within the context of sterile neutrino oscillations.

2.1.2 3-flavor neutrino oscillations

The most general scenario of neutrino oscillations within the standard model involves mixing between the three flavor states ν_α; electron neutrino ν_e, muon neutrino ν_μ and tau neutrino ν_τ respectively, these flavor states are related to the mass eigenstates $\nu_i = (\nu_1, \nu_2, \nu_3)$ by means of a unitary 3×3 matrix known as the PMNS (Pontecorvo-Maki-Nakagawa-Sakata) [28, 29] mixing matrix

$$|\nu_\alpha\rangle = U_{\mathsf{PMNS}} |\nu_i\rangle \ . \tag{23}$$

In the Particle Data Group (PDG) [32] parameterization, the PMNS matrix for Dirac type neutrinos is given by

$$\begin{aligned} U_{\mathsf{PMNS}} &= \begin{pmatrix} U_{e1} & U_{e2} & U_{e3} \\ U_{\mu 1} & U_{\mu 2} & U_{\mu 3} \\ U_{\tau 1} & U_{\tau 2} & U_{\tau 3} \end{pmatrix} = R(\theta_{23}) U(\theta_{13}, \delta) R(\theta_{12}) = U^{\mathsf{PDG}}, \\ U^{\mathsf{PDG}} &= \begin{pmatrix} c_{12}c_{13} & c_{13}s_{12} & e^{-i\delta}s_{13} \\ -c_{23}s_{12} - c_{12}e^{i\delta}s_{13}s_{23} & c_{12}c_{23} - e^{i\delta}s_{12}s_{13}s_{23} & c_{13}s_{23} \\ s_{12}s_{23} - c_{12}c_{23}e^{i\delta}s_{13} & -c_{12}s_{23} - c_{23}e^{i\delta}s_{12}s_{13} & c_{13}c_{23} \end{pmatrix}, \end{aligned} \tag{24}$$

where $R(\theta_{23})$ and $R(\theta_{12})$ are 3×3 orthogonal matrices in the (23) and (12) planes respectively and $U(\theta_{13}, \delta)$ is a 3×3 unitary matrix in the (13) plane generated from the basis of the three

neutrino mass eigenstates. In this manner, it is more convenient to interpret the data from the different atmospheric, terrestrial, reactor and solar neutrino experiments; the parameter δ shown in Eq. 24 is a phase related to the degree of charge conjugation and parity (CP) violation *i.e.* a quantitative measure of how matter and antimatter are in disproportion. The probability for a neutrino starting with a well defined flavor eigenstate ν_α and further observed as flavor species ν_β after traveling a particular distance L in *vacuum* and having energy E can be expressed as:

$$\begin{aligned} P_{\alpha\beta} = \delta_{\alpha\beta} - 4\sum_{i>j} \mathcal{R}\Big[U^*_{\alpha i}U_{\alpha j}U_{\beta i}U^*_{\beta j}\Big] \sin^2\big(1.27\Delta m^2_{ij}\frac{L}{E}\big) \\ + 2\sum_{i>j} \mathcal{I}\Big[U^*_{\alpha i}U_{\alpha j}U_{\beta i}U^*_{\beta j}\Big] \sin\big(2.54\Delta m^2_{ij}\frac{L}{E}\big), \end{aligned} \tag{25}$$

where the $U_{\alpha i}$ [5] correspond to the elements of the PMNS mixing matrix, E is the neutrino energy, L is the (beam or source) to detector distance and $\Delta m^2_{ij} = m^2_i - m^2_j$ are the squared mass splittings between the neutrino mass eigenstates ν_1, ν_2, ν_3.

Closed analytical forms to describe the oscillation probabilities with three flavors are somehow cumbersome. However, since $\Delta m^2_{21} \ll \Delta m^2_{31}$, oscillation transitions in atmospheric and terrestrial experiments can be written as crude approximation; see, e.g., Refs. [33, 34]

- $P_{\nu_e\to\nu_\mu} \simeq \sin^2 2\theta_{13}\sin^2\theta_{23}\sin^2\left(\frac{1.27\Delta m^2_{31}L}{E_\nu}\right)$
- $P_{\nu_e\to\nu_\tau} \simeq \sin^2 2\theta_{13}\cos^2\theta_{23}\sin^2\left(\frac{1.27\Delta m^2_{31}L}{E_\nu}\right)$
- $P_{\nu_\mu\to\nu_\mu} \simeq 1 - \sin^2 2\theta_{13}\sin^2\theta_{23}\sin^2\left(\frac{1.27\Delta m^2_{31}L}{E_\nu}\right)$.

In further sections Sec. [4, 6] we will discuss sterile neutrino oscillations. For the neutrino energies available and for the baselines that we will consider, oscillations among the three neutrinos of the standard model are negligible.

[5] The index α corresponds the flavor states (e, μ, τ) whereas the index $i = (1, 2, 3)$ corresponds to the mass states.

2.2 Neutrino Oscillation in matter

In 1985 S. Mikheyev and A. Smirnov [35], based on previous work by L. Wolfenstein [36] pointed out that matter can modify neutrino oscillations, the so called Mikheyev-Smirnov-Wolfestein (MSW effect) that is crucial to the study and understanding of solar neutrinos. The MSW effect allows for adiabatic transitions among the neutrinos due to the rich interactions with the electron media in the Sun, resulting in a large mixing angle which is in agreement with results from the KamLAND experiment [37]. Our Sun is a main-sequence star in the hydrogen-burning stage, whose overall reaction that produces around 95% of the energy arising from the fusion of protons into a helium nucleus [38]

$$4p \rightarrow \mathrm{He}^{2+} + 2e^{+} + 2\nu_e \ . \tag{26}$$

The two remaining positrons further annihilate with two electrons in the medium producing

$$4p + 2e^{-} \rightarrow \mathrm{He}^{2+} + 2\nu_e + 26.7 \text{ MeV}. \tag{27}$$

In addition, the produced neutrinos reach the Earth from the solar fusion without practically any absorption. This propagation of neutrinos in matter is analogous to that of light when reaches a different index of refraction other than vacuum. The interaction of electrons with matter change the energy levels of the neutrino mass eigenstates via charged current interactions of neutrinos with electrons. This implies that neutrinos in matter have a different mass than those in vacuum and since neutrino oscillations are driven by the mass states, the oscillation effect is different. Furthermore, if the density profile of matter changes, there could exist a resonant effect that enhances flavor transitions between neutrinos [35, 36].

In perspective, an effective two flavor neutrino oscillation in vacuum is described by the Hamiltonian:

$$H_f = \frac{\Delta m_{21}^2}{4E} \begin{pmatrix} -\cos 2\theta_{12} & \sin 2\theta_{12} \\ \sin 2\theta_{12} & \cos 2\theta_{12} \end{pmatrix}, \tag{28}$$

then, considering matter effects (neutrino-electron scattering) we add an effective potential in the form of

$$V_M = \begin{pmatrix} \pm\sqrt{2}G_F N_e & 0 \\ 0 & 0 \end{pmatrix}, \tag{29}$$

where G_F is the Fermi coupling constant and N_e is the corresponding number density of electrons [35]. Hence, now the Hamiltonian ($H_m = H_f + V_M$) expresses the evolution in the presence of matter, this mechanism resembles that of the two flavor neutrino oscillation in

vacuum developed in Sec. 2.1.1. Furthermore, the probability of having an electron neutrino in the source and detected as a muon neutrino is

$$P_{e\mu} = 1 - \sin^2 2\theta_m \sin^2 \left(1.27\Delta\tilde{m}^2 \frac{L}{E}\right), \tag{30}$$

now the angle θ_m has contribution from the effective potential V_M and $\Delta\tilde{m}^2$ is the mass difference in matter. In units where the baseline $[L] = \mathrm{m}$, the mass splitting $[\Delta\tilde{m}^2] = \mathrm{eV}^2$ and the neutrino energy $[E] = \mathrm{MeV}$, there is a factor of 1.27 that gives the conversion into these particular units. In further sections Sec. [4, 6] we will discuss sterile neutrino oscillations. However, at the baselines that we are considering there, matter effects are muted.

2.3 Current Status of Experimental Values

Up to date, almost all the oscillation parameters have been established by past and present neutrino experiments. Each of these experiments contribute in measuring a specific parameter. For instance, the KamLAND experiment [37] played a crucial role in determining the solar parameters θ_{12} and Δm^2_{21}. In addition, recent assessments of the experimental neutrino data set from nuclear reactors had established the non-vanishing reactor mixing angle (θ_{13}); see, e.g., Refs. [39, 40, 41]. Moreover, the standard three neutrino oscillation data set has been determined, in the form of the neutrino mass squared differences, Δm^2_{21} and $|\Delta m^2_{31}|$ as well as the corresponding three mixing angles; θ_{12}, θ_{13} and θ_{23} respectively. Furthermore, there exists evidence of a non-zero Dirac CP-violating phase presented by the NOνA [42] and T2K [43] collaborations. The best fit for the Dirac phase δ obtained by Salas *et al.* [12] is consistent with δ=1.08π (1.58π) for normal (inverted) ordering [6] respectively.

Present-day global fits of the standard three neutrino oscillation picture are described in Refs. [12, 44], a summary from the analysis performed by the authors of Ref. [12] is presented in Tab. 1

[6]The label NO or IO stands for normal and inverted ordering respectively. The normal ordering (NO) imply that the ν_1 mass state is the lightest with $\nu_1 < \nu_2 < \nu_3$ contrary to the inverted ordering (IO) where the ν_3 mass state is the lightest instead.

parameter	best fit $\pm 1\sigma$	2σ range	3σ range
Δm^2_{21} $[10^{-5}\mathrm{eV}^2]$	$7.50^{+0.22}_{-0.20}$	7.12−7.93	6.94−8.14
$\lvert\Delta m^2_{31}\rvert$ $[10^{-3}\mathrm{eV}^2]$ (NO)	$2.55^{+0.02}_{-0.03}$	2.49−2.60	2.47−2.63
$\lvert\Delta m^2_{31}\rvert$ $[10^{-3}\mathrm{eV}^2]$ (IO)	$2.45^{+0.02}_{-0.03}$	2.39−2.50	2.37−2.53
$\sin^2\theta_{12}/10^{-1}$	3.18 ± 0.16	2.86−3.52	2.71−3.69
$\theta_{12}/^\circ$	34.3 ± 1.0	32.3−36.4	31.4−37.4
$\sin^2\theta_{23}/10^{-1}$ (NO)	5.74 ± 0.14	5.41−5.99	4.34−6.10
$\theta_{23}/^\circ$ (NO)	49.26 ± 0.79	47.37−50.71	41.20−51.33
$\sin^2\theta_{23}/10^{-1}$ (IO)	$5.78^{+0.10}_{-0.17}$	5.41−5.98	4.33−6.08
$\theta_{23}/^\circ$ (IO)	$49.46\ ^{+0.60}_{-0.97}$	47.35−50.67	41.16−51.25
$\sin^2\theta_{13}/10^{-1}$ (NO)	$2.200\ ^{+0.069}_{-0.062}$	2.069−2.337	2.000−2.405
$\theta_{13}/^\circ$ (NO)	$8.53\ ^{+0.13}_{-0.12}$	8.27−8.79	8.13−8.92
$\sin^2\theta_{13}/10^{-1}$ (IO)	$2.225\ ^{+0.064}_{-0.070}$	2.086−2.356	2.018−2.424
$\theta_{13}/^\circ$ (IO)	$8.58\ ^{+0.12}_{-0.14}$	8.30−8.83	8.17−8.96
δ/π (NO)	$1.08\ ^{+0.13}_{-0.12}$	0.84−1.42	0.71−1.99
$\delta/^\circ$ (NO)	$194\ ^{+0.24}_{-0.22}$	152−255	128−359
δ/π (IO)	$1.58\ ^{+0.15}_{-0.16}$	1.26−1.85	1.11−1.96
$\delta/^\circ$ (IO)	$284\ ^{+0.26}_{-0.28}$	226−332	200−353

Table 1: Relevant standard neutrino oscillation parameters adapted from Ref. [12].

3 Sterile neutrinos

3.1 Introduction

The Standard Model of particle physics is a theoretical framework that describes three of the four fundamental forces of nature namely; weak, strong and electromagnetic in a unified way. The fundamental particles are classified into *quarks* and *leptons*, and their interactions are mediated by *bosons*. The former are confined in doublets of *quark-antiquark*, known as *mesons* (kaons, pions) and in triplets forming *baryons* (neutrons, protons), these mesons and baryons are called *hadrons*. In general, quarks experience the four fundamental forces of nature, on the other hand, leptons do not interact via the strong force. There exists six different varieties of *quarks*: *up* (u), *down* (d), *charm* (c), *strange* (s), *top* (t) and *bottom* (b). Similarly, leptons are grouped in doublets with a neutral particle and a charged particle:

electron (e) and *electron neutrino* (ν_e); *muon* (μ) and *muon neutrino* (ν_μ); *tau* (τ) and *tau neutrino* (ν_τ). Furthermore, the *gluons* (g) are the bosonic particles that participate in the strong force via interactions with quarks. The weak bosons interact with both quarks and leptons via electroweak processes and there are three of them; two charged bosons $W^\pm$ and a neutral one, the Z^0 boson. The last piece of the particle content in standard model is the Higgs boson, postulated by P. Higgs, F. Englert and R. Brout [45, 46] and discovered by the ATLAS [47] and CMS [48] collaborations respectively. In the standard model neutrinos are massless; therefore, neutrino oscillations represents an evidence for physics beyond the standard model.

3.2 Beyond three neutrino oscillations

There exist persistent hints from different experiments, notably the Liquid Scintillator Neutrino Detector (LSND) [1] and the Booster Neutrino Experiment (MiniBooNE) [2], as well as reactor and gallium experiments [3, 49, 50, 9, 5] that may indicate the existence of a fourth neutrino species, a light sterile neutrino ν_s with a mass of $\mathcal{O}(1)$ eV mixing with active neutrinos, in a similar fashion as the effective two-neutrino oscillation probability in vacuum discussed on (Sec.2.1, Eq. 21). For a comprehensive review on global sterile neutrino oscillations see *e.g.* [51] and references therein. While sterile neutrino oscillation would be a simple explanation, if applied to both the ν_μ-appearance results (LSND, MiniBooNE) and the reactor indications, it also would predict the disappearance of ν_μ, which has not been observed.

In searches of new physics via sterile neutrino oscillations [52], the parameter space generated by the mixing angle $\sin^2 2\theta$ and the mass splitting Δm^2 has to be determined. Hence, selecting a proper combination of baseline and neutrino energy is fundamental. For instance, in such experiments, we should account for an optimal value of the parameter L/E_ν in the oscillatory phase from the two-flavor neutrino oscillation probability. [7] However, if the combination of the parameter L/E_ν is much greater than the mass splitting Δm^2, in consequence, oscillations might appear quickly. Since neutrino experiments have limited length L and energy E_ν resolution, the oscillatory term averages out to 1/2 for values of $\Delta m^2 \gg L/E_\nu$. Therefore, the sensitivity to the mass splitting Δm^2 is muted. Furthermore, since the oscillation probability is a function of the mixing angle; $\sin^2 2\theta$, if this parameter is expected to be small, hence the experiment would require high statistics to observe the

[7] Recall the model discussed in Sec.2.1, Eq. 21

elusive signal.

In the LSND experiment, the anomaly aroused from the electron anti-neutrino appearance channel $\bar{\nu}_\mu \to \bar{\nu}_e$, pointed out towards a Δm^2 of ~ 1 eV^2 with a statistical significance of 3.8σ. The experiment used the decay-at-rest (DAR) of hadrons (π^+, π^-) arising from the collision of a 800 MeV beam of protons on target, the resulting pions; π^+, further decay into muons μ^+ which were stopped, producing neutrino fluxes, $\bar{\nu}_\mu$ and ν_e respectively. The resulting neutrinos were observed in the detector at a distance $L \sim$ 30 m from the beam dump [1]. Moreover, the signature of the expected anti-neutrinos $\bar{\nu}_e$ was detected via inverse beta decay

$$\bar{\nu}_e + p \to e^+ + n, \tag{31}$$

which results in a prompt signal from the positron and a delayed scintillation light arising from the neutron capture on hydrogen.

At the LSND experiment, the fraction of the baseline to energy L/E_ν [m/MeV] is of the order $\mathcal{O}(1)$. Therefore, from a two flavor neutrino oscillation, this experiment should be sensitive to values of $\Delta m^2 \geq 0.1$ eV^2. Actually, the oscillation probability measured by the LSND experiment was consistent with $(2.64 \pm 0.67 \pm 0.45) \times 10^{-3}$ [1]. In summary, the experiment observed an excess of ~ 88 events over the expected backgrounds. While the LSND was a single detector experiment, for instance the SciBooNE/MiniBooNE experiment is a two detector design searching for evidence in the $(\bar{\nu}_\mu \to \bar{\nu}_\mu)$ channel, the setup of this experiment is useful in cases where the neutrino flux is not well constrained, a common feature in decay-in-flight (DIF) type of beams. In such experiments, accelerated protons are driven a onto target where hadrons are produced (π, K). The charged hadrons are then focused towards a decay pipe where the selected pions and kaons further decay into muons generating the corresponding muon neutrino flux.

The MiniBooNE experiment is located at a distance of 540 m from the beam target at Fermilab, it comes in a sphere shape detector of 800 ton filled with mineral oil. In this experiment, the events were detected using the Cerenkov light related to the leaving particles. Moreover, the Cerenkov light formed rings, the surplus of light and ring geometry were used to determine both, the direction and particle energies [53]. In MiniBooNE, the quantity L/E [m/MeV] is of the order $\mathcal{O}(1)$ consistent with the LSND experiment. Overall, the MiniBooNE experiment observed a ν_e excess of 381.2 ± 85.2 events Ref. [2].

As part of the complementary program for searches of sterile neutrino oscillations, the KARMEN [54], ICARUS [55], and NOMAD [56] experiments searched for a sterile neutrino in the $\nu_\mu \to \nu_e$ oscillation channel, setting exclusion limits but not within the sensitivity

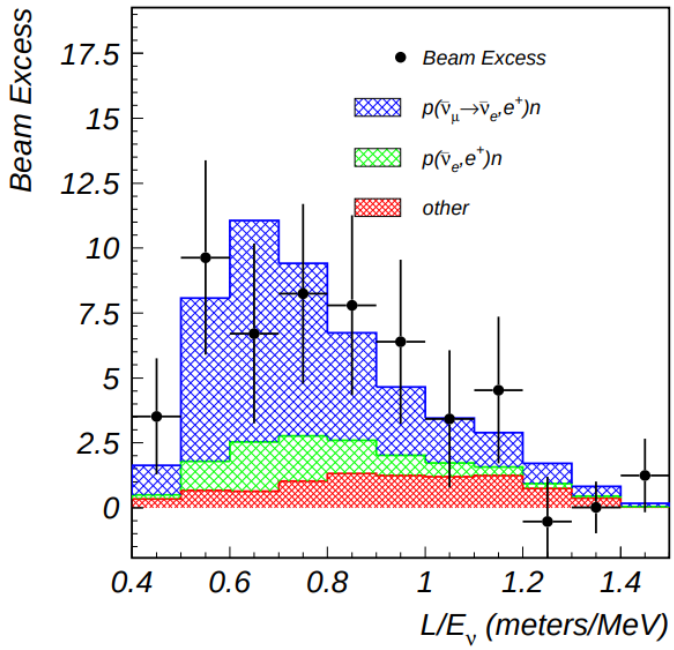

Figure 1: Adapted from Ref. [1], the LSND excess ($\bar{\nu}_\mu \to \bar{\nu}_e$). Green and red histograms depict the backgrounds from the intrinsic anti-neutrinos $\bar{\nu}_e$ in the beam and other related sources, in accordance. The blue histogram represents a possible $\bar{\nu}_\mu \to \bar{\nu}_e$ event. This potential signal is mapped to the sensitivity in the $(\Delta m^2, \sin^2 2\theta)$-plane.

reach to entirely disprove the LSND and MiniBooNE signals.

In addition to the previous experimental hints of a sterile neutrino by the LSND and MiniBooNE, another set of anomalous results came from anti-neutrino beams produced by reactors known as the "Reactor Anti-neutrino Anomaly" (RAA) [3], that employs a comparison between the measured rate of electron anti-neutrino events from nuclear reactors compared to the predictions. Nuclear reactors at commercial and research cores are the main sources of neutrinos were the rate anomaly was observed. These neutrinos are produced trough the fission of the isotopes: ^{235}U, ^{238}U, ^{239}Pu and ^{241}Pu. The theoretical predictions of anti-neutrino rates are obtained by a convolution of the corresponding anti-neutrino fluxes with the inverse beta decay cross section, with energies ranging from 1.8 MeV to 8 MeV. However, an absolute prediction of the neutrino fluxes; see, e.g., Refs. [57, 3] is challenging

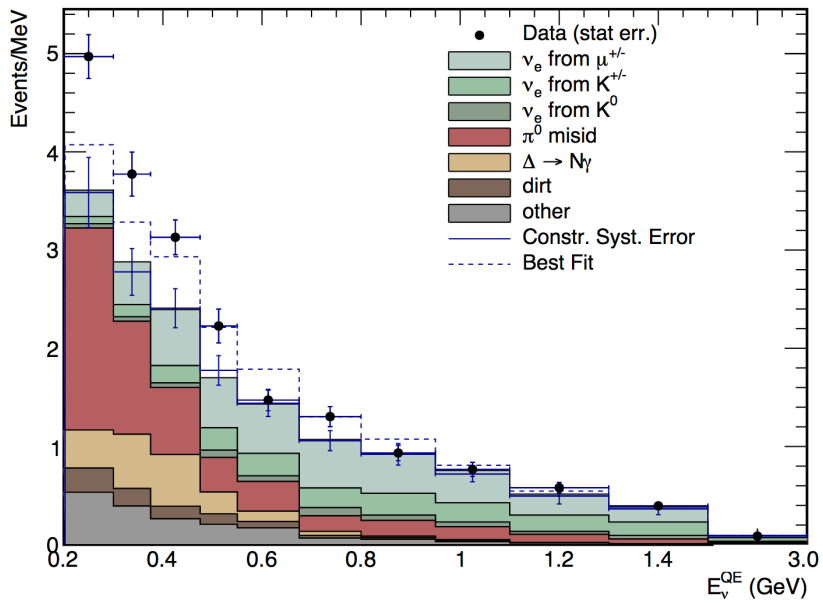

Figure 2: Adapted from Ref. [2], the neutrino energy E_ν distribution for signal ν_e events and backgrounds with $12.84\times\ 10^{20}$ PoT.

to implement due to several production mechanisms of electron anti-neutrinos from the beta decay of the corresponding fission fragments. In summary, the measured ratios point towards $R_{obs}/R_{pred} \simeq 0.933 \pm 0.021$ with a 3.2σ statistical significance as shown by the authors of Ref. [3]. In further sections we invoke the sterile neutrino hypothesis as a plausible explanation for the RAA.

Last but not least, experiments using radio-chemical sources like SAGE (Soviet-American Gallium Experiment) [58], and GALLEX (GALLium EXperiment) [59], found less ν_e events than the expected on a 60 ton and 30 ton gallium detectors respectively via inverse beta decay reaction

$$\nu_e +^{71}\text{Ga} \rightarrow e^- +^{71}\text{Ge}. \tag{32}$$

Such discrepancy if explained as sterile neutrino oscillations would imply a 2.3σ statistical significance as pointed out in Ref. [5], with a ratio $R_{obs}/R_{pred} = 0.84\pm0.05$ which is commonly referred as the "gallium anomaly". This anomaly is merely theoretically driven and could

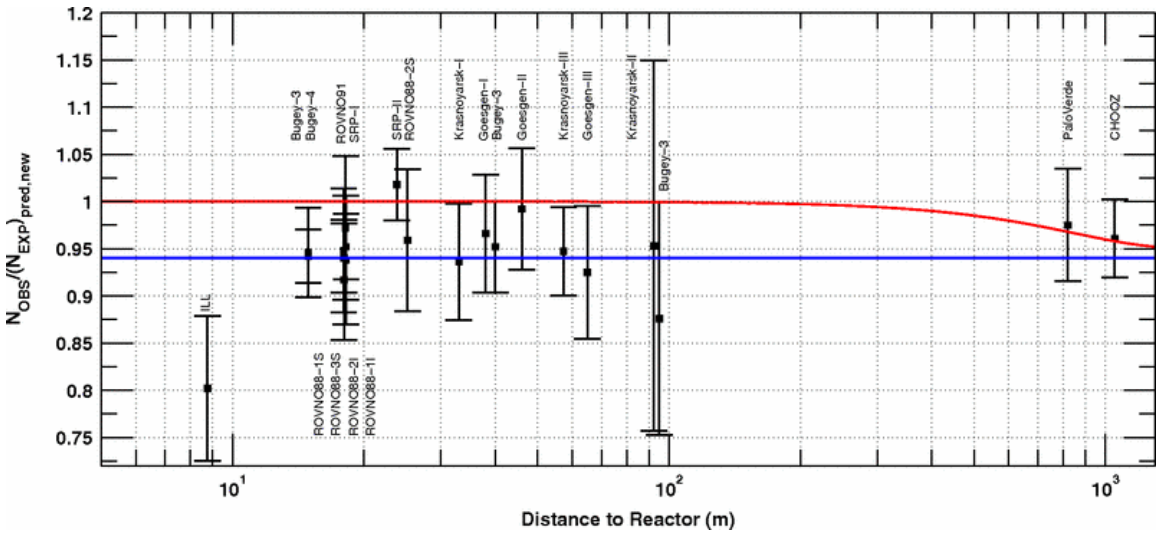

Figure 3: Adapted from Ref. [3]. Depiction of the short baseline reactor anti-neutrino anomaly (RAA). The red line represents the fit with a non-zero value of θ_{13}, the blue line is the mean of the ratios.

be due to an overestimation of the transition rates to the excited states.

Further models that include a second or third sterile neutrino could explain those anomalous results but we are not discussing them in this thesis since in general the fits do not improve significantly with respect to the single sterile neutrino oscillation fit as pointed out by the authors of Ref. [51]. Moreover, the addition of an extra neutrino state in the standard model has salient repercussions beyond those established by three neutrino oscillation framework. It has been pointed out in the literature that a light sterile neutrino is in tension with bounds from cosmological observations [60, 61, 62, 63]. Furthermore, if a light sterile neutrino exists in nature, imprints of this particle could be observed at the KATRIN experiment [64] by noticing a bump in the inverse beta decay spectrum from the associated Curie plot.

4 Sterile neutrino searches at ENUBET

4.1 Introduction

This section is based on our findings from Ref. [65]. For this work, I was involved in the calculations of the results from all the sections, the interpretations and ideas were mostly guided by Prof. Dr. Huber. Furthermore, I wrote the first draft version of the manuscript. Prof. Dr. Huber went over the document editing what ended up to be the final manuscript version submitted to the journal.

A recent example of a proposal to build a tagged kaon beam is the ENUBET (Enhanced NeUtrino BEams from kaon Tagging) beam-line technology [66] based on the reconstruction of positrons from the three-body semi-leptonic $K^+ \to e^+\nu_e\pi^0$ decay, aimed to determine the absolute ν_e/ν_μ flux at 1% level.

The basis for this type of tagged beam is a conventional narrow band beam with a short transfer line $\sim 20\,\mathrm{m}$ followed by a $40\,\mathrm{m}$ long decay tunnel surrounded by positron detectors [67]. Primary protons of 120 GeV in energy are impinged on a fixed target to generate hadrons (π, K) which are caught, selected according to their charge and transported further down to the instrumented decay tunnel with a momentum spread of roughly $\pm 20\%$ centered at 8.5 GeV [66]. The positrons are identified inside the decay tunnel by calorimetric routines, the beam-line is optimized to enhance the ν_e-component from the three-body semi-leptonic decay and significantly reduce the beam ν_e-background arising from the muon decays [66]: the decay tunnel is too short for muon decays to produce a significant fraction of muon neutrinos. In ENUBET, the rate of positrons provides a direct measurement of the ν_e produced in the tunnel. Also the three-body decay of the kaon produces a wider neutrino energy distribution than the two-body decay of the pion, $\pi^+ \to \mu^+ + \nu_\mu$, as can be seen in Fig. 4, thus a energy cut can be used to effectively control any remaining backgrounds after tagging. Neutrinos from this type of source will oscillate as usual, since the precision of neither the time nor the energy measurement on the positron will allow to determine the mass eigenstate produced and thus all that tagging does is to fix the beam normalization and baseline travelled.

4.2 Experimental framework

The predicted event rates were calculated based on neutrino fluxes provided by the ENUBET collaboration [66, 68]. We consider a 1kt liquid argon detector with energy resolution which

follows a normal distribution with a width of $\sigma(E) = 17\%/\sqrt{E[\mathrm{GeV}]}$ for electrons and $\sigma(E) = 10\%/\sqrt{E[\mathrm{GeV}]}$ for muons, respectively. The energy window is consider between the interval of [0-10] GeV with a total of 50 bins (uniformly spread), in accordance with [67, 68]. All calculations are performed with GLoBES [69, 70] using the N-flavor oscillation engine of Refs. [71, 72].

The signal events are obtained via the survival probability of the electron neutrinos stemming from the K^+ in the beam that decay into $e^+ + \nu_e$, which then interact in the liquid argon detector. The yields of kaons transported to the entrance of the decay tunnel is 1.69×10^{-3} K^+/PoT (protons on target) for 120 GeV protons. The tagged ν_e-flux is assumed to be 99% pure.

The largest source of beam related background in the detector is due to neutral current coherent π^0 production: The π^0 decays into two photons. For pion energies below $\sim 1\,\mathrm{GeV}$ the opening angle is large enough to cleanly reconstruct both photons and thus no confusion with a ν_e charged current event arises. At higher energies, however, the two photons are more collinear and may no longer be reconstructed as two particles, hence these neutral currents events may be misidentified as charged current ν_e events. Liquid Argon (LAr) detectors have very fine granularity and as a result very good particle identification. In particular photon-induced showers can be recognized by the separation among the vertex and the start of the shower. Without going into the details of event reconstruction, we estimate the rate of coherent, π^0 production. The cross section for neutral current coherent π^0 production has been measured by MINOS on iron [73] and by NOvA on carbon [74]; we use a theory-derived scaling factor of $(A/12)^{2/3}$ to translate these results for argon in accordance with the Berger-Sehgal model [75]. Expected π^0 rates were found to be of order 0.1% compared to our signal ν_e events and thus can be neglected for this analysis. The beam normalization is know at the 1%-level due to the high kaon tagging efficiency [66].

Similarly, muon neutrinos can be selected at the neutrino detector using radius-energy correlations. We performed a 5 GeV energy cut to avoid contributions from un-tagged π^+; because the branching ratio for the semi-leptonic decay $K^+ \to e^+\nu_e\pi^0$ is well known, 5%, and the number of kaon decays in this mode is fixed by tagging, we can use the equally well-know branching ratios for the muon neutrino generating decay modes $K^+ \to \mu^+\nu_\mu$ (60%) and $K^+ \to \mu^+\nu_\mu\pi^0$ (3%) to know the muon neutrino flux with the same accuracy as the electron neutrino flux. Final states here are charged current ν_μ interactions with the detector. As in the electron neutrino case, the neutral current related background events were found to be of order 0.1% compared to signal and thus, negligible.

Placing a 1 kt liquid argon detector at a distance of 1 km from the decay pipe we obtain 1,568 ν_e events and 24,603 ν_μ events/year[8]. Detection efficiencies in this type of detector are close 100% and for simplicity we neglect them, a simple increase of running time or detector mass by 10-20% will be required to compensate for this approximation. For a few-GeV beam, a distance of $L = 1$km yields $L/E_\nu \simeq 0.2$ [km/GeV], which corresponds to an oscillation with $\Delta m^2 \simeq 5\,\mathrm{eV}^2$. The ν_μ energy E_ν spectrum crests at roughly 7 GeV, while the ν_e energy spectrum peaks around 4 GeV as shown in Fig. 4.

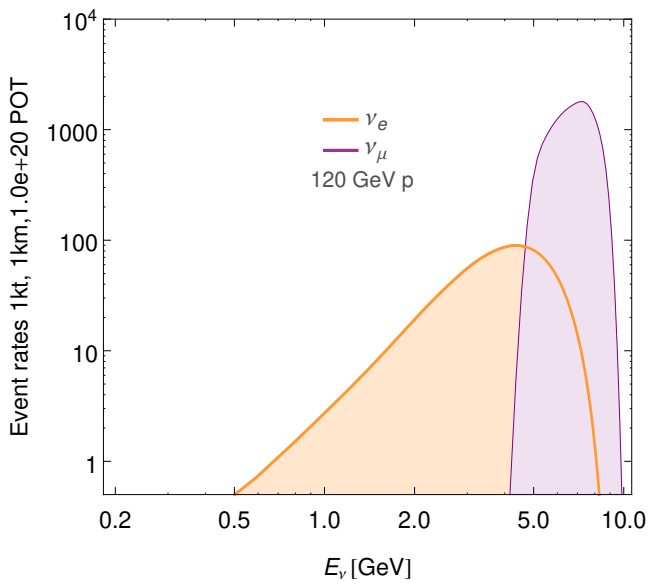

Figure 4: Expected event rates assuming a 1kt liquid argon detector at baseline $L = 1$km for 120 GeV protons with a power beam of 10^{20} PoT/yr.

We do not include the appearance channels in our analysis and have confirmed that their inclusion would not impact our results in an appreciable manner.

[8]This includes cuts on the beam radius with acceptances of 24% for ν_e and 34% for ν_μ, respectively [76].

4.3 Analysis

Our study is based on the 3+1 framework of neutrino oscillations (3-flavor states and 1-sterile state), from which we follow the leptonic mixing matrix parameterization from Ref. [51]

$$U = R(\theta_{34})\tilde{U}(\theta_{24}, \delta_{24})R(\theta_{14})R(\theta_{23})\tilde{U}(\theta_{13}, \delta)\tilde{U}(\theta_{12}, \delta_{12}), \tag{33}$$

were $R(\theta_{i,j})$ are orthogonal 4×4 matrices on the (i, j)-plane, $\tilde{U}(\theta_{i,j}, \delta_{i,j})$ are 4×4 unitary matrices on the (i, j)-plane and δ is the standard Dirac CP violating phase, under the short baseline approximation all extra phases are zero *i.e.* there will be no additional CP violation in the $3 + 1$ scenario. Furthermore, the probability for a neutrino produced in the flavor eigenstate ν_α and being observed as flavor ν_β after moving a particular distance L in *vacuum* with definite energy E is:

$$\begin{aligned} P_{\alpha\beta} = \delta_{\alpha\beta} - 4\sum_{i>j} \mathcal{R}\Big[U^*_{\alpha i}U_{\alpha j}U_{\beta i}U^*_{\beta j}\Big] \sin^2\big(1.27\Delta m^2_{ij}\frac{L}{E}\big) \\ + 2\sum_{i>j} \mathcal{I}\Big[U^*_{\alpha i}U_{\alpha j}U_{\beta i}U^*_{\beta j}\Big] \sin\big(2.54\Delta m^2_{ij}\frac{L}{E}\big), \end{aligned} \tag{34}$$

where $U_{\beta j}$ $(\beta = e, \mu, \tau, s; j = 1, 2, 3, 4)$ correspond to the entries of the 4×4 mixing matrix Eq. 33, E is the neutrino energy, L is the beam to detector distance, $\Delta m^2_{ij} = m^2_i - m^2_j$ are the squared mass splittings between the standard neutrino mass eigenstates ν_1, ν_2, ν_3 and a ν_4 sterile state. Based on our simulated charged current event rates and assuming a 10^{20} PoT/yr beam power on a 1kt LAr detector, we obtain sensitivities for the hypothesis of sterile neutrino oscillation under a (3+1) scenario assuming five years of beam operation. Interpreting the ENUBET experimental data set in terms of sterile neutrino oscillations allows to test large values of Δm^2_{41} and relatively sizable mixing between ν_e and ν_s states. This corresponds well with the parameter space regions indicated by the gallium results [5], Neutrino-4 results [77] and IceCube results [6, 7]. Sensitivity contours were calculated based[9] on the $\Delta\chi^2$ value for each parameter pair (Δm^2_{41}, $\sin^2 2\theta_{14}$) and by determining the boundary of the corresponding exclusion/allowed regions by translating the $\Delta\chi^2$ to confidence levels assuming a χ^2 function with two degrees of freedom (d.o.f.) and the remaining parameters fixed according to Tab. 2.

For a recent discussion about the limitations of Wilks' theorem in disappearance searches with free beam normalization see Ref. [78], which is not quite the same case as considered

[9] Assuming Normal Ordering (NO).

Table 2: Relevant oscillation parameters used in this analysis.

standard PMNS	value [**NO**]	sterile parameter	value
θ_{12}	$33.2°$	δ_{24}	0
θ_{23}	$45°$	δ_{12}	0
θ_{13}	$9°$	θ_{34}	0
Δm^2_{21} $[10^{-5}\text{eV}^2]$	7.5	θ_{24}	free
$\lvert\Delta m^2_{31}\rvert$ $[10^{-3}\text{eV}^2]$	2.6	θ_{14}	free
δ	0	Δm^2_{41} $[10^{-1}{-}10^{2}\text{eV}^2]$	free

here, but gives an indication of the size of the resulting corrections. We consider different null hypotheses H_0:

- H_0: no oscillation. We compute data assuming no disappearance and fit the resulting Asimov data set with finite value of Δm^2 and $\sin^2 2\theta$. The result is a sensitivity limit, shown as dashed lines.

- H_0: oscillation according the Reactor Anti-neutrino Anomaly (RAA) best fit. We compute data assuming the best fit of the RAA is true and fit the resulting Asimov data set with different value of Δm^2 and $\sin^2 2\theta$. The result are allowed regions (with closed contours), shown as solid lines.

- H_0: oscillation according the Neutrino-4 best fit. We compute data assuming the best fit of Neutrino-4 is true and fit the resulting Asimov data set with different value of Δm^2 and $\sin^2 2\theta$. The result are allowed regions (with closed contours), shown as solid lines.

- H_0: oscillation according the IceCube best fit. We compute data assuming the best fit of IceCube is true and fit the resulting Asimov data set with different value of Δm^2 and $\sin^2 2\theta$. The result are allowed regions (with closed contours), shown as solid lines.

For all cases we consider a combined fit of muon and electron neutrino disappearance and profile over the not-shown θ_{i4} mixing angles. In this type of beams, the normalization error of the signal becomes important, while the beam flux is very well know due to tagging the signal charged current cross sections suffer from significant uncertainties. We assume, that the main physics program of ENUBET, which are cross section measurements, have reduced

the resulting effective signal uncertainty to either 1%, 2% or 5%, where we take 2% as default unless stated otherwise.

4.4 Results

The effective two-flavor limit in the electron disappearance channel yields this simple oscillation probability:

$$P_{ee} = 1 - 4|U_{e4}|^2\big(1 - |U_{e4}|^2\big)\sin^2\big(1.27\Delta m^2_{41}\frac{L}{E}\big), \tag{35}$$

and according to the parameterization Eq.(33) this case reduces to the effective two flavor oscillation.

$$P_{ee} = 1 - \sin^2 2\theta_{ee}\sin^2\big(1.27\Delta m^2_{41}\frac{L}{E}\big), \tag{36}$$

where $\sin^2 2\theta_{ee} = 4|U_{e4}|^2\big(1 - |U_{e4}|^2\big)$ and $\theta_{ee} = \theta_{14}$ is the angle that encodes mixing. Figure [5] shows our projection for the sterile neutrino oscillation sensitivity at ENUBET in the $\sin^2 2\theta_{ee}$-Δm^2_{41} plane at 99% C.L. for an exposure of 1 kt assuming five years of beam operation. The blue, magenta and red dashed-dotted lines account for 1%, 2% and 5% signal normalization systematic. Also shown the 1σ, 2σ, 3σ preferred regions for the best fit RAA [3] and Neutrino-4 [4] assuming 2% signal normalization systematic.

Until recent results from IceCube [6, 7] no indication for sterile neutrino oscillation in the muon disappearance channel had been found. The IceCube experiment collected a total of 305,735 events in both ν_μ and $\bar{\nu}_\mu$ mode to search for sterile neutrinos with energies in the interval between [500, 9976] GeV; the collaboration found allowed close contours at 90% C.L. near the best fit point at $\Delta m^2_{41} = 4.5$ eV^2 and $\sin^2 2\theta_{24} = 0.1$ respectively. It will be interesting to see how global analysis of the sterile neutrino data-sets could be modified by including the IceCube findings and if the tension among the disappearance and appearance channels remains. For our analysis of ν_μ disappearance at ENUBET, in the 3+1 scenario with short baseline approximation, the muon neutrino disappearance probability can be expressed

$$\begin{aligned} P_{\mu\mu} &= 1 - 4|U_{\mu4}|^2\big(1 - |U_{\mu4}|^2\big)\sin^2\big(1.27\Delta m^2_{41}\frac{L}{E}\big) \\ &= 1 - \sin^2 2\theta_{\mu\mu}\sin^2\big(1.27\Delta m^2_{41}\frac{L}{E}\big), \end{aligned} \tag{37}$$

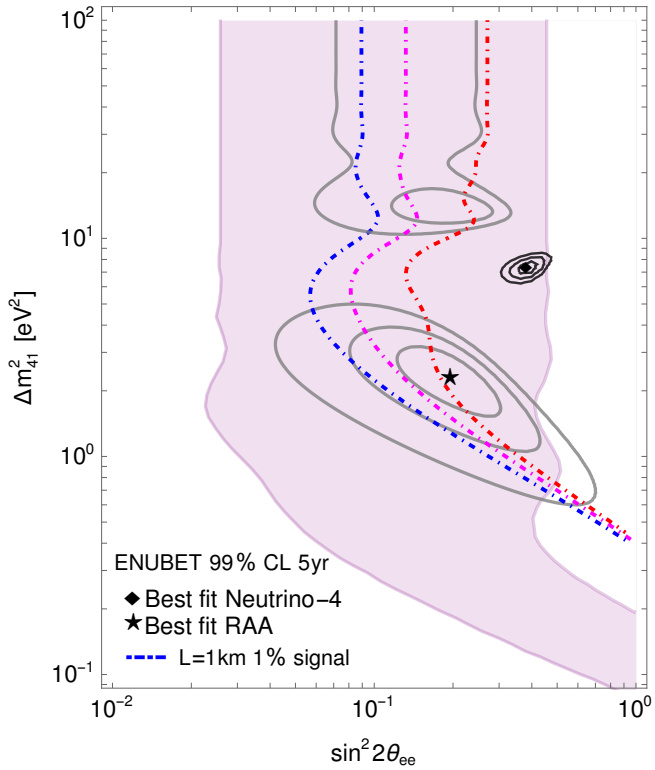

Figure 5: Comparison of the expected sensitivities in the $\sin^2 2\theta_{ee}$-Δm^2_{41} plane. The blue, magenta and red dashed-dotted lines corresponds to a 1%, 2% and 5% signal systematic uncertainties at baseline length of $L = 1$km. The black diamond point represents the best fit point from Neutrino-4 [4], star represents the best fit of the reactor anti-neutrino anomaly RAA [3]. In addition we show 90% C.L. allowed region (purple shaded area) of the gallium anomaly JUN45 [5].

where $|U_{\mu 4}| = \cos\theta_{14}\sin\theta_{24}$ and the effective mixing angle $\theta_{\mu\mu}$ depends on both θ_{14} and θ_{24}

$$\sin^2 2\theta_{\mu\mu} = 4\cos^2\theta_{14}\sin^2\theta_{24}\big(1 - \cos^2\theta_{14}\sin^2\theta_{24}\big). \tag{38}$$

Figure [6] shows the sterile neutrino oscillation sensitivity at ENUBET in the $\sin^2 2\theta_{24}$-Δm^2_{41} plane at 99% C.L. for an exposure of 1 kt assuming five years of beam operation. The

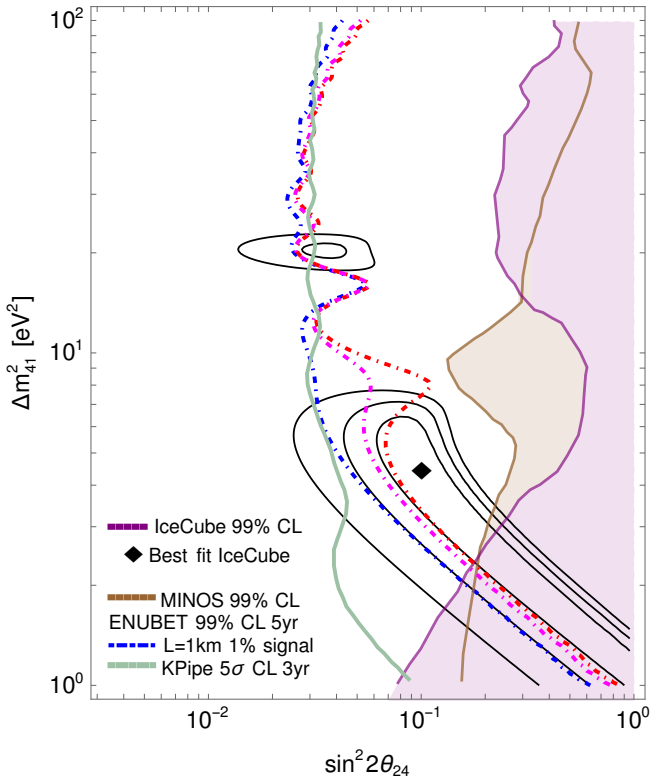

Figure 6: Comparison of the expected sensitivities in the $\sin^2 2\theta_{24}$-Δm^2_{41} plane ($\sin^2 2\theta_{\mu\mu} \approx \sin^2 2\theta_{24}$). The blue, magenta and red dashed-dotted lines corresponds to a 1%, 2% and 5% signal systematic uncertainties at baseline length of $L = 1$km. The black diamond point represents the best fit point 90% C.L. from IceCube [6, 7], shaded purple/brown areas are excluded by IceCube and MINOS [8] respectively.

blue, magenta and red dashed-dotted lines account for 1%, 2% and 5% signal normalization systematic. Also shown the 1σ, 2σ, 3σ preferred regions assuming 2% signal normalization systematic for true $\sin^2 2\theta_{24} = 0.1$ and $\Delta m^2_{41} = 4.5$ eV^2 from IceCube [6, 7]. For comparison we also show the sensitivity of another kaon decay based proposal, called Kpipe [79]: Kpipe is a proposed experiment to investigate sterile neutrinos from kaon decay at rest and is aimed to set the strongest limits in the muon neutrino disappearance channel. The expected

number of ν_μ events is 1.02×10^5 events/year in a 684 ton liquid scintillator detector, which comes in the shape of 120 m long pipe. Kpipe would have about an order of magnitude more signal events than the proposal we consider here and thus in principle has the potential to provide excellent sensitivity in this channel.

5 Sterile neutrinos at nuclear reactors

5.1 Introduction

Reactors at both *commercial* and *research* facilities are the main sources of terrestrial electron anti-neutrinos $\bar{\nu}_e$, derived from nuclear fission and radioactive decays. The salient difference between commercial and research cores is that the former is much larger than the latter; commercial cores are therefore much more powerful and produce a larger flux of anti-neutrinos. Reactor neutrino experiments are in principle disappearance experiments since the anti-neutrinos produced are not energetic enough to produce neither muon nor tau neutrinos. The production of neutrinos comes primarily from the fission of the four isotopes: ^{235}U, ^{238}U, ^{239}Pu and ^{241}Pu at more than 99%. Furthermore, reactor anti-neutrinos are produced at a rate of $\mathcal{O}(10^{21})$ decays per second per GW$_{th}$[10] providing a clean signal via inverse beta decay (IBD). As an exemplification, characteristic IBD events are detected as a double coincident signal, a prompt signal produced by the positron ionisation and further annihilation in the detector. This time coincidences in the signal help to reduce radioactive backgrounds. Since the energy of the position can be determined in the IBD process, the $\bar{\nu}_e$ energy is determined by kinematic relations: $E_\nu \approx E_e + m_e + 0.78$ MeV.

5.2 Non-zero θ_{13} from nuclear reactors

Ever since the Savannah River nuclear reactor experiment in 1956 [15], a numerous amount of reactor experiments have been constructed to investigate the spectrum of neutrinos from IBD reactions at various distance from the source. More recently, reactor neutrino experiments were designed to probe the third neutrino mixing angle θ_{13}. The first experiment built to measure the θ_{13} mixing angle was the CHOOZ experiment [80], this power plant station ran at a mean power of 8.5 GW$_{th}$, located at around 1 km from the core. The CHOOZ experiment found no evidence of neutrino oscillations and set a limit on $\sin^2 2\theta_{13} < 0.12$ at 90% C.L. [80]. Similar case for the Palo Verde experiment [81], letting this sector of the three flavor neutrino oscillation mixing parameters inconclusive.

After the limits set up by CHOOZ and Palo Verde and without conclusive evidence for non-zero θ_{13} mixing angle, the neutrino physics community proposed to build a new set of experiments to measure the θ_{13} mixing angle, that culminated with the construction

[10] Gigawatt of thermal power.

and successful measurement at the Double CHOOZ [39], Daya Bay [40] and RENO [41] experiments. An improvement with respect to the old experiments was the use of multiple detectors to reduce the uncertainties in the predicted fluxes of $\bar{\nu}_e$ emitted from the sources. The Double CHOOZ experiment consisted of both, near and far detectors placed at distances around 400 m and 1 km respectively, with a 8.3 ton detector mass each operating at a nuclear power plant with two 4.25 GW_{th} reactors. The Daya Bay experiment consist of three different locations with eight detector modules total; two near detectors located at around 360 m and 560 m of distance and a far detector close to 1.9 km from the nuclear plant of six 2.9 GW_{th} thermal power reactors. The RENO experiment observed the disappearance of electron anti-neutrinos from a nuclear plant consisted of six reactors with a thermal power of 2.8 GW_{th} each, with two copies of detectors deployed at 294 m and 1383 m from the core, respectively. Current global fits see *e.g.* [12] report a best-fit value for the reactor mixing angle $\theta_{13} = 8.53°(8.58°)$ for normal (inverted) ordering respectively, (primarily driven by the Daya Bay measurement) as shown in table 1.

5.3 Present searches of light sterile neutrinos at nuclear reactors

Searches of sterile neutrinos at both (*commercial* and *research*) reactors started to gain attention in the neutrino physics community after the disagreement between observed and predicted reactor anti-neutrino fluxes [57, 3], known as "Reactor Anti-neutrino Anomaly" (RAA). Such anomalous results could be consistent with those observed at the LSND and MiniBooNE experiments as well. Moreover, these discrepancies can be explained in a simple way by the addition of a sterile neutrino that mixes with the neutrino flavor states via the inclusion of an effective two flavor neutrino oscillation in a similar fashion as the model described in Sec. 2.1.1. The sterile neutrino hypothesis requires the inclusion of a mass splitting $\Delta m^2 \simeq 1\ \mathrm{eV}^2$ with a mixing angle such that $\sin^2 2\theta \lesssim 0.1$, which is driven predominantly by recent searches at the commercial reactors DANSS and NEOS [50, 49].

For instance, the authors of Ref. [9] performed a combined fit of the DANSS and NEOS experimental data in search for sterile neutrinos. In Fig. 7, the C.L. contours derived from the analysis are depicted; 95% in dark green, 99% in green and 99.9% in light green respectively. If interpreted as oscillations, this results in a 3.3σ significance, although the sterile neutrino hypothesis is favored, it is not yet conclusive [9]. For a review on the status of global fits with a light sterile neutrino from different experiments see, Refs. [51, 9, 82].

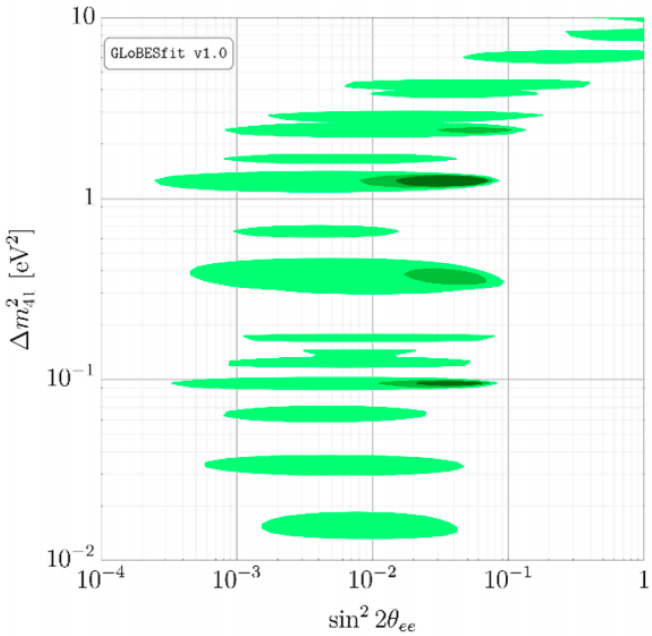

Figure 7: Adapted from Ref. [9]. The C.L. contours derived from a combined analysis of DANSS and NEOS; in dark green is shown the 95% C.L., the 99% C.L. is displayed in green and the 99.9% C.L. is depicted in light green.

6 Future searches for light sterile neutrinos at nuclear reactors

6.1 Introduction

This section is based on Ref. [83]. In this part of the thesis we will discuss some aspects regarding prospective ways to search for a light sterile neutrino in nuclear reactors at both commercial and research cores. In this work, I was involved in the calculations of the green field studies and sensitivity to sterile neutrinos at TAO sections. Furthermore, I wrote the TAO section of the draft. Dr. Berryman was the main investigator of this project, involved in the calculations of all the sections of the paper, he wrote the green field studies and lithium sensitivity sections of the draft. Prof. Dr. Huber guided all the calculations and

interpretations of the results, he wrote the introduction and conclusion sections of the draft. In addition Prof. Dr. Huber went over the final version of the draft editing what ended up to be the document submitted to the journal.

As far as upcoming neutrino experiments are concerned, the JUNO experiment will set the most precise measurement of the neutrino parameters θ_{12} and Δm^2_{21} as well as determine the mass ordering [84]. In preparation to the measurement of the θ_{13} mixing angle, the question of how to predict the reactor anti-neutrino spectrum gained renewed attention [85, 57] and the surprising result was an upward correction to the predicted inverse beta decay (IBD) event rate by approximately 6%. Which is commonly known in the literature as the reactor anti-neutrino anomaly (RAA) [3], this would be naturally explained if the $\bar{\nu}_e$ mixed with an additional species of neutrino with a mixing angle $\sin^2 2\theta \simeq 0.1$ and $\Delta m^2 \geq 1\,\mathrm{eV}^2$. For a review of the status of the field at that time, see Ref. [86]. For a comprehensive experiment-specific fit status of sterile neutrino oscillations, see Ref. [87].

Moving into reactor neutrino experiments, modern experiments (i.e., those conducted after 2011) all rely on a comparison of measured event rate spectra at different baselines and are thus *independent* of flux predictions. Nonetheless, reactor flux predictions have been subject to intense study (for a summary, see Refs. [88, 9]). Moreover, the rate anomaly has not, as yet, been resolved, though it may be less significant than originally suggested[11]. The spectral anomaly known as the 5 MeV bump is entirely unresolved but is likely not due to new physics [90]. The experiments we will be discussing here will contribute data on neutrino fluxes, but this is not a focus of our work. Instead, we ask the question what the best possible experiment using reactor neutrinos would look like to find a light sterile neutrino or to exclude a sizable mixing. We also focus exclusively on electron anti-neutrinos and their potential mixing with a sterile neutrino. This choice is motivated, to some degree, by the fact that all data on the $\nu_e \to \nu_e$ and $\bar{\nu}_e \to \bar{\nu}_e$ channels at this point are mutually consistent. The same cannot be said of the $\nu_\mu \to \nu_e$ and $\overline{\nu}_\mu \to \overline{\nu}_e$ data sets; additionally, the global disappearance data are known to be inconsistent with the global appearance data when interpreted in the context of a truly sterile fourth neutrino [51, 82]. Our hope and motivation for this study is that a carefully analysis of neutrino disappearance at reactors will facilitate future analyses of the global neutrino data set.

There are three main reasons in selecting electron neutrinos[12] from nuclear reactors as

[11] A recent work [89], if confirmed, would provide a simple and consistent solution to the RAA by shifting the ratio of plutonium-239 to uranium-235 in the integral beta spectra. In this case, beta data, neutrino data, summation and conversion calculations all would be in good agreement.

[12] We consider only electron flavor neutrinos and/or anti-neutrinos and we rely on context to disambiguate

the source of choice, namely:

1. They are free, in the sense that they are constructed for purposes other than neutrino physics.

2. They are very bright, with experimentally accessible fluxes of up to $10^{13}\,\mathrm{cm}^{-2}\,\mathrm{s}^{-1}$.

3. They produce anti-neutrinos which can be cleanly detected via IBD, which both provides a flavor tag and has a large[13] cross section of approximately $6 \times 10^{-43}\,\mathrm{cm}^2$ per fission.

For instance, other sources of electron neutrinos which have been considered for sterile neutrino searches include radioactive sources [91, 92], beta-beams [93], kaon beams [65], beam-driven beta-decay sources [94] and stored muon beams [95]. None of these other electron neutrino sources shares all of the advantages of nuclear reactors, in particular they all would be pretty expensive and require detectors much larger than what will be considered in this study. On the other hand, some of these approaches like beam-driven, beta-decay sources and stored muon beams would yield far better sensitivities than those at reactor neutrino experiments. But what sensitivities are possible with a reactor source? This is the subject to explore in the former analysis.

6.2 Green Field studies

For the neutrino energies available at nuclear reactors and for the baselines that we will consider (up to 100 meters), oscillations among the three neutrinos of the Standard Model are negligible. Therefore, if a sterile neutrino[14] exists and participates in oscillations, then any oscillations observed over these distances would be attributable to the new state. We may describe these oscillations in the two-flavor limit, writing the $\overline{\nu}_e$ survival probability as

$$P_{\overline{e}\overline{e}} = 1 - \sin^2 2\theta \sin^2 \left(\frac{1.27 \Delta m^2 L}{E_\nu} \right). \tag{1}$$

In this particular model, L is the baseline over which the neutrinos propagate (given in meters [m]) and E_ν is their energy in [MeV]. The parameter Δm^2 is the difference in the

these two cases.

[13] Relative to other weak-interaction processes.

[14] We will use the term "sterile" neutrino to refer to a generic fourth neutrino that participates in oscillations but not in weak interactions.

squares of the masses of two neutrino mass eigenstates; $\sin^2 2\theta$ is the mixing angle describing the amplitude of the oscillations. Probing sterile neutrinos amounts to determining $\sin^2 2\theta$ and Δm^2.

The main goal of this study is to determine the optimal configuration(s) for a two-baseline reactor neutrino experiment with realistic operational assumptions. We categorize these by the class of reactor at which they are conducted, at either a *commercial* or a *research* reactor facility. The salient difference between these is that the former is much larger than the latter; commercial cores are also more powerful and produce a larger flux of anti-neutrinos. However, the layout of the facilities at which these are housed prevents an experiment from operating within a certain distance of the core, typically of the order 10-25 m. Research cores, though less powerful, are less constrained in this regard: one can operate an experiment as close as 3-6 m from the core. The increase in flux from the shorter allowed baseline partially offsets the lower absolute rate of anti-neutrino production. We consider for each of these scenarios in turn.

6.2.1 Methodology

We consider pseudo-experiments in which the spectrum of reactor anti-neutrinos is observed at two baselines. We treat the detector as point-like, but the reactor core has finite physical extent; we treat the latter as a perfect sphere. Because of this, we cannot use the oscillation probability in Eq. (1) as is, we must flux-average the probability $P_{\overline{ee}}$ over the production region. The effect of this is to average out high-frequency oscillations: if the oscillation wavelength is comparable to or smaller than the size of the production region, then the experiment will have no sensitivity to the associated value of Δm^2. Details on this procedure and the resulting average survival probability are given in Appendix A.1.

The analysis window is taken to be $E_{\text{prompt}} \subset [2.0, 8.0]$ MeV; we generally assume a bin size of 250 keV, but occasionally consider finer spacing; for instance in Sec. 6.4 a bin size of 100 keV is used instead. We assume a constant, nonzero background in each energy bin, ignoring any systematic uncertainty on this background and assuming that the near and far baselines experience the same background rate per unit exposure. We consider two energy response models as limiting cases of the detector resolution. The first is the response model of the PROSPECT experiment, which the collaboration has provided in the Supplemental Material to Ref. [96]. The response may be approximately described as a Gaussian with width $\sim 7\%/\sqrt{E/\ [\text{MeV}]}$, albeit including a non-Gaussian tail at low energies. On the other hand is the upcoming Taishan Antineutrino Observatory (TAO) experiment [11], for which

the resolution is taken to be of the order $\sim 1\%/\sqrt{E\ [\mathrm{MeV}]}$. We assume that the TAO detector response is perfectly Gaussian.

For a given experimental configuration, specified by the near and far baselines (L_{near} and L_{far}, respectively), we form the following χ^2 function:

$$\begin{aligned}\chi^2 = &\sum_i^{N_{\mathrm{bins}}} \left(\frac{M_i^N - \phi_i P_i^N \left(\sin^2 2\theta, \Delta m^2, \{\eta_j\}\right)}{\sigma_i^N} \right)^2 \\ &+ \sum_i^{N_{\mathrm{bins}}} \left(\frac{M_i^F - \phi_i P_i^F \left(\sin^2 2\theta, \Delta m^2, \{\eta_j\}\right)}{\sigma_i^F} \right)^2 \\ &+ \sum_j^{N_{\mathrm{sys}}} \left(\frac{\eta_j}{\sigma_j} \right)^2 \end{aligned} \tag{2}$$

The components of this expression are as follows:

- The M_i^N and M_i^F represent the numbers of pseudo-data IBD counts in energy bin i in the near and far detectors, respectively. These pseudo-data are generated without oscillations.

- The P_i^N and P_i^F are the predicted numbers of events in energy bin i for oscillation parameters $\{\sin^2 2\theta,\ \Delta m^2\}$ and nuisance parameters $\{\eta_j\}$, which we discuss more below.

- The σ_i^N and σ_i^F are the statistical uncertainties associated with the predictions. We account for the nonzero background by defining the corresponding σ_i^N and σ_i^F; we write

$$\sigma_i^{N,F} = \sqrt{P_i^{N,F} + 2B_i^{N,F}}, \tag{3}$$

  where B_i^N (B_i^F) is the number of background events per energy bin in the near (far) detector.[15]

- The ϕ_i are nuisance parameters for the flux in each energy bin. Our analysis is *flux free* in that we do not introduce a prior on these nuisance parameters; while we use

[15] The factor of 2 in Eq. (3) arises because the counts are background-subtracted. The expected number of raw events in each bin is $P_i^{N,F} + B_i^{N,F}$; subtracting the background increases the statistical error by another factor of $B_i^{N,F}$.

the Huber-Mueller flux model [85, 57] to generate our pseudo-data, our analysis is not sensitive to this choice. These unconstrained nuisance parameters reduce the number of degrees of freedom in the fit, leading to lower values of the χ^2 and, ultimately, less statistical significance. However, sensitivities derived in this fashion are more robust than those that rely on a given flux model. We may analytically minimize the χ^2 with respect to these nuisance parameters to obtain

$$\phi_i = \frac{\dfrac{M_i^N P_i^N}{(\sigma_i^N)^2} + \dfrac{M_i^F P_i^F}{(\sigma_i^F)^2}}{\left(\dfrac{P_i^N}{\sigma_i^N}\right)^2 + \left(\dfrac{P_i^F}{\sigma_i^F}\right)^2}. \tag{4}$$

- Lastly, the $\{\eta_j\}$ are the nuisance parameters describing our systematic uncertainties, which are assumed to be consistent with the systematic uncertainties described by the STEREO collaboration [97]:
  - A 1.2% uncorrelated normalization uncertainty.
  - A 1.0% uncorrelated energy scale uncertainty.
  - A 0.3% correlated energy scale uncertainty.

  We expect this to characterize the capabilities of next-generation reactor experiments. We ignore the possibility of uncorrelated systematic uncertainties in the measured spectral shape in our initial studies; we discuss this further in Sec. 6.2.5.

We only consider simple $\Delta\chi^2$ statistics here. Although recently, it has been repeatedly emphasized that searches for sterile neutrino oscillations do not satisfy Wilks' theorem: simple $\Delta\chi^2$ statistics do not provide the proper coverage in the $\sin^2 2\theta$–Δm^2 parameter space, so converting $\Delta\chi^2$ values to confidence levels using Gaussian statistics is formally incorrect (see, e.g., Refs. [98, 78]). Consequently, we avoid rigorously assigning confidence levels. That said, statistical methods that aim to address these deficiencies (e.g., the CL_s method [99] and Feldman-Cousins method [100]) are computationally intensive; performing these at scale is beyond the scope of this work. Therefore, we present our sensitivities as contour(s) along which $\Delta\chi^2 = 11.83$ — for 2 degrees of freedom, this would correspond to 3σ if Wilk's theorem applied. In most cases, the true significance will be less than this.

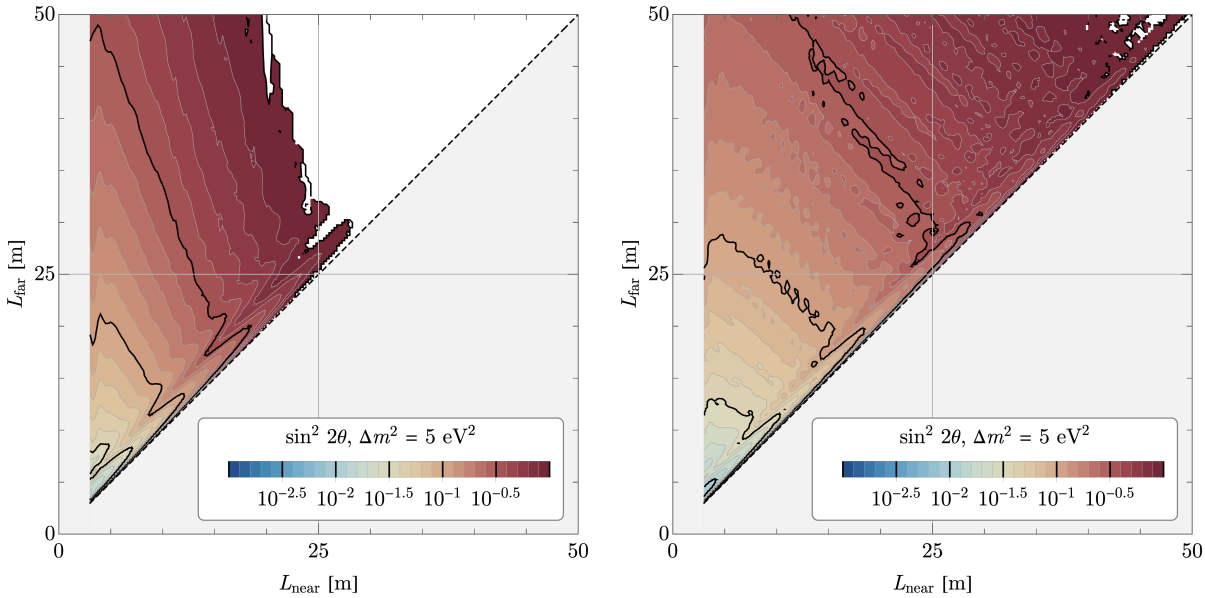

(a) (b)

Figure 8: The sensitivity ($\Delta\chi^2 = 11.83$) of a hypothetical two-baseline research reactor experiment to oscillations with $\Delta m^2 = 5$ eV^2 as a function of its near and far baselines, L_{near} and L_{far}. Panel (a) shows results for PROSPECT-like response, while panel (b) shows results for TAO-like response.

6.2.2 Research Reactor Optimization

We begin with research reactors. Because of their smaller size and because they are not attached to the heat-extraction apparatus of a commercial core, one could operate an experiment with much shorter baselines at a research core. For instance, the MINER experiment [101] can to operate within 1-3 m of a low-power (1 $\mathrm{MW_{th}}$) reactor. However, it is more typical of the current generation of short-baseline experiments to operate in the range 6-10 m. We consider baselines as close as 3 m and as far as 50 m from a core whose radius is taken to be 20 cm and whose power is set to 100 $\mathrm{MW_{th}}$. The total exposure is fixed at one year, which we assume corresponds to 90 days of reactor-on time. Moreover, because research reactors use high-enriched uranium fuel, the flux of anti-neutrinos is entirely attributable ^{235}U fission.

The drawback of operating so close to the core is backgrounds. On one hand, operating close to the core subjects the detector to reactor-correlated neutron and gamma backgrounds. On the other, the detector is necessarily close to the surface subjecting the detector to cosmogenic backgrounds. It is possible to mitigate either source of background, but this presents a fundamental challenge to the operation of such an experiment. We will assume that a background rate of 250 events per ton-day of reactor-on time spread uniformly over the analysis region at both detector sites. This is broadly consistent with the background rate achieved at PROSPECT [96].

In Figs. 8a and 8b, we show representative sensitivities to oscillations with $\Delta m^2 = 5$ eV^2 for a PROSPECT-like and TAO-like detector response, respectively. The color conveys the sensitivity ($\Delta\chi^2 = 11.83$) to $\sin^2 2\theta$ for each pair of near and far baselines; white space indicates baseline pairs for which there is no sensitivity. The central conclusion is that getting as close as possible to the reactor core is the key factor in improving the sensitivity. Note that even in the case of a detector with TAO-like energy resolution, the sensitivity barely reaches $\sin^2 2\theta \sim \mathcal{O}(10^{-2})$ for the closest conceivable baseline of 3 m. Constructing an experiment this close to a core would be fantastically challenging; it would be more reasonable to limit the near baseline to ~ 6 m. In this case, the optimal sensitivity worsens slightly to $\sin^2 2\theta \sim 3 \times 10^{-2}$.

6.2.3 Commercial Reactor Optimization

Commercial reactors are several orders of magnitude more powerful than research reactors, meaning that one does not need to operate an experiment at as short a baseline to have

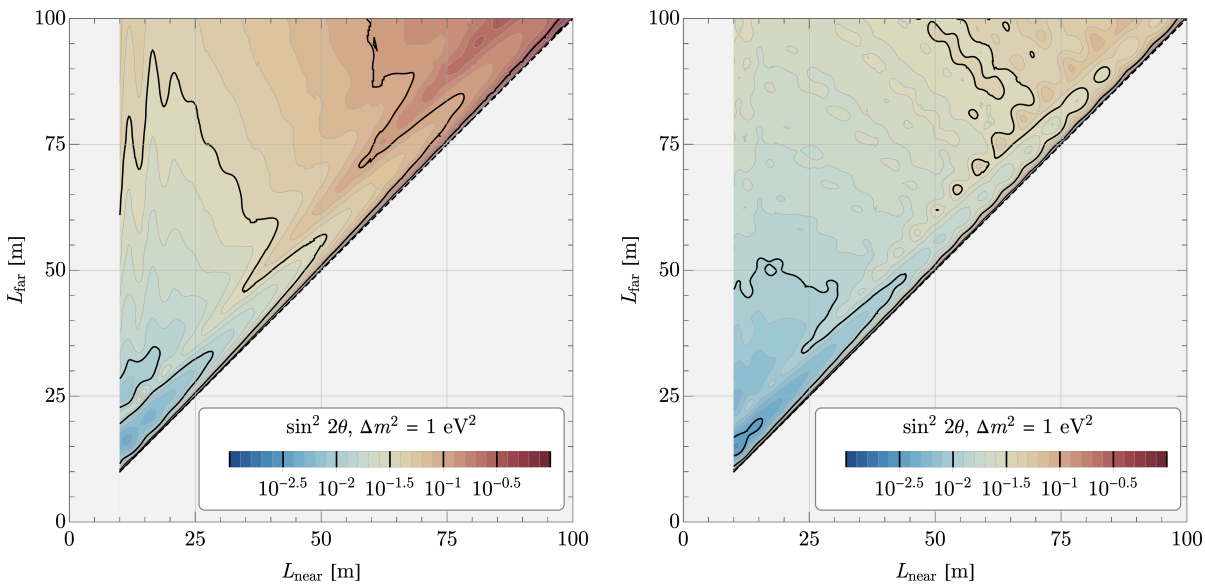

Figure 9: The sensitivity ($\Delta\chi^2 = 11.83$) of a hypothetical two-baseline commercial reactor experiment to oscillations with $\Delta m^2 = 1$ eV^2 as a function of its near and far baselines, $L_{\rm near}$ and $L_{\rm far}$. Panel (a) shows results for PROSPECT-like response, while panel (b) shows results for TAO-like response.

an appreciable event rate. This is an advantage, since one *cannot* conduct an experiment at such close baselines, given the complicated layout of commercial reactor plants. We take the radius of the core to be 2.0 m, the core power to be 4.5 $\mathrm{GW_{th}}$ and the exposure to be one year, which we assume corresponds to 365 days of reactor-on time. Moreover, the fuel at commercial reactors is typically low-enriched uranium, meaning the anti-neutrino flux is a nontrivial combination of the fluxes from the four main fissile isotopes (^{235}U, ^{238}U, ^{239}Pu, ^{241}Pu). We take the following values for the effective isotopic fission fractions:

$$\left\{^{235}\mathrm{U},\, ^{238}\mathrm{U},\, ^{239}\mathrm{Pu},\, ^{241}\mathrm{Pu}\right\} = \{0.56,\, 0.07,\, 0.31,\, 0.06\}\,.$$

The closest baseline that any experiment has attained at a commercial reactor is ~ 10 m at DANSS experiment [102], the result of the specific construction of the facility at which it is housed. A more typical scenario is akin to the NEOS experiment [49], which is located at a distance of approximately 24 m from a commercial core at the Hanbit Power Plant. We consider baselines between 10-100 m in our simulations. The impact of this lack of closeness on sterile neutrino searches is twofold. Firstly, because shorter baselines allow for searches for larger oscillation frequencies, the sensitivity of commercial reactor experiments to larger values of Δm^2 will be muted. However, the larger core size also causes high-frequency oscillations to average out anyways, so the main advantage lost is in the event rate. Secondly, because the experiment is further from the core, the backgrounds are less severe: reactor-correlated neutron and gamma backgrounds are substantially attenuated and higher overburdens can be achieved to reduce cosmogenic backgrounds. We assume a background rate of 90 events per ton-day of reactor-on time, roughly corresponding to the background rate measured at NEOS [49].

In Figs. 9a and 9b, we show sensitivities to oscillations with $\Delta m^2 = 1$ eV^2. The color scale is the same as in Figs. 8a and 8b; the sensitivity is improved for commercial reactors over research reactors, owing to the much larger event rate. As before, the key factor in determining the sensitivity is allowing for as short a baseline as achievable, subject to the constraints of the facility. The best sensitivity shown for the TAO-like response corresponds to $\sin^2 2\theta \sim 3 \times 10^{-3}$, but even restricting the baselines to be no less than 25 m or using the PROSPECT response model (or both) yields a maximum sensitivity better than $\sin^2 2\theta \sim 10^{-2}$ for this value of Δm^2.

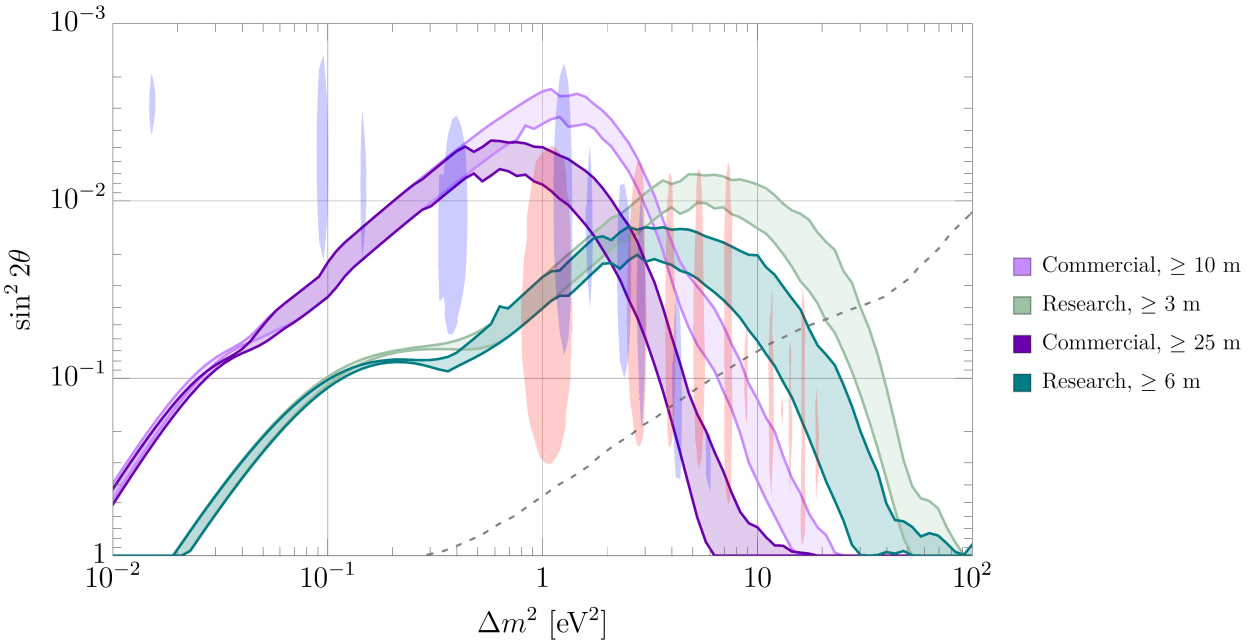

Figure 10: The baseline-optimized sensitivity ($\Delta\chi^2 = 11.83$) to $\sin^2 2\theta$ as a function of Δm^2. The purple (green) curves are for a commercial (research) reactor. The lighter band of either color represents the sensitivity with optimistic assumptions about the possible closest baseline; the darker bands represent more realistic assumptions. The weakest (strongest) sensitivity of each color corresponds to a PROSPECT-like (TAO-like) energy resolution. Also shown is the 95% C.L. sensitivity from KATRIN (dashed gray), as well as the 3σ-preferred regions from Neutrino-4 [10] (red) and from the global analysis of Ref. [9] (blue).

6.2.4 Comparisons

We aggregate our results for both the commercial and research reactor cases in Fig. 10. The figure shows the baseline-optimized sensitivity ($\Delta\chi^2 = 11.83$) to $\sin^2 2\theta$ particular to a given Δm^2. We note that there is no achievable configuration that maximizes the sensitivity at every such value. The purple curves correspond to commercial reactors, whereas green curves are for research reactors. The lighter shade of either color exploits the full range of baselines, i.e., that a detector can be placed as close as possible to a given type of core (10 m for commercial, 3 m for research). The darker shade, in contrast, truncates the

nearest baseline at what we believe is a more realistic distance (25 m for commercial, 6 m for research). The shading indicates the effect of the detector resolution, ranging between the PROSPECT (lower) and TAO (upper) responses.

For a fixed exposure, the sensitivity of a commercial reactor experiment exceeds that of a research reactor experiment by some $\mathcal{O}(1-10)$ factor, a consequence of the increased statistics at commercial experiments. However these experiments are most sensitive to oscillations with different values of Δm^2, a consequence of the different core sizes and permissible baselines. If one were optimizing a sterile neutrino search for $\Delta m^2 \lesssim 2-3$ eV^2, then one would ultimately elect to operate the experiment at a commercial reactor; conversely, for larger values of Δm^2, one would choose a research reactor. This figure concretely demonstrates the benefit of putting the detector closer to the core for probing high-frequency oscillations — a transition occurs around $\Delta m^2 \sim 0.5$ eV^2 (~ 2 eV^2) for commercial (research) reactors where the advantage of higher statistics and shorter baselines dissipates.

To contextualize these sensitivities, we also show the projected final 95% C.L. sensitivity of the ongoing KATRIN tritium-decay experiment [103] in dashed gray. While a research core would be the preferred method up to $\Delta m^2 \sim 30$ eV^2 if one could realize ultra short baselines, KATRIN is ostensibly the preferred technique for searches above $\Delta m^2 \sim 15$ eV^2 for more realistic configurations. However, there is an important caveat in interpreting the KATRIN sensitivity: this depends on the prior on the effective neutrino mass-squared, m_ν^2, that one extracts from the experiment. If one insists that $m_\nu^2 \geq 0$ – a sensible physical criterion – then one derives the sensitivity shown in the figure. If one were to allow m_ν^2 to take any value – positive or negative – to avoid a biased measurement, then the resulting sensitivity changes; this is depicted in Fig. 3 of Ref. [103] for the exclusion based on current data. We are unaware of any study of this effect on the ultimate sensitivity of KATRIN and do not attempt one here, but this suggests that the constraint may not be robust below $\Delta m^2 \sim 30$ eV^2. If this is the case, then research reactor experiments may be the best path forward to exploring this portion of the parameter space.

The last two components of Fig. 10 are the regions of parameter space preferred by analyses of separate existing data sets. The first is the 3σ-preferred region from an analysis of the Neutrino-4 experiment [10], shown in red shading. The second is the 3σ-preferred[16] region from a recent global analysis of Bugey-3, DANSS, Daya Bay, Double Chooz, NEOS and RENO from Ref. [9], shown in blue shading. These are the regions that next-generation reactor experiments will target — indeed, the presence of closed 3σ contours in existing

[16] What this reference calls "3σ" should more appropriately be called the "$\Delta\chi^2 = 11.83$" exclusion.

analyses is what inspires the next generation of experiments in the first place. Our results suggest that the optimal strategy to probe these regions would be to build a commercial reactor experiment to probe below $\Delta m^2 \sim 2$ eV^2 and a research reactor experiment to probe above this, and that they should both be as close as can be achieved to their respective cores.

We have considered the effect of bin size on Fig. 10. Specifically, we have looked at bins of width 100 keV for both a PROSPECT-like and TAO-like response model at both a commercial and research reactor facility. On one hand, smaller bin sizes result in fewer events in each bin, leading to poorer statistical uncertainties; on the other, smaller bin sizes afford sensitivity to higher oscillation frequencies, assuming the energy resolution is adequate to resolve these. The sensitivity increases slightly for high Δm^2 for the TAO-like response because of this latter consideration; the sensitivity slightly decreases for a PROSPECT-like response because of the worsening statistical uncertainties. On balance, these changes are not markedly different from Fig. 10. We have also investigated the effect of 30-keV bins on analyses with our TAO-like response and find no appreciable gain in sensitivity.

6.2.5 Exposure and Systematics Limitation

One can ask how the sensitivities shown in Fig. 10 can be improved by either operating the experiment for a longer period of time or by constructing a more massive detector. To study this, we must include an effect that we have ignored to this point. While our flux-free analysis does not introduce any prior uncertainties on the flux, one should account for systematic uncertainties on the measured spectral shape, in addition to the systematics that we have already included. We assume that this systematic is uncorrelated between energy bins and that next-generation experiments can achieve shape uncertainties as low as 0.5%, consistent with the value claimed by TAO [11]. This is introduced to our χ^2 in Eq. (2) via the replacement

$$\left(\sigma_i^{N,F}\right)^2 \to \left(\sigma_i^{N,F}\right)^2 + (P_i^{N,F}\sigma_{\rm sh})^2, \tag{5}$$

where $\sigma_{\rm sh}$ represents the shape systematic.

We consider a pseudoexperiment at a research reactor with a near baseline of 6 m and a far baseline of 9 m, roughly corresponding to the near and far baselines at PROSPECT, and that employs the TAO response model. In Fig. 11, we show the sensitivity to $\sin^2 2\theta$ for fixed values of Δm^2 – 1 eV^2 in cyan and 5 eV^2 in magenta – as a function of exposure. The vertical, gray line corresponds to the 5 ton-years exposure used in our previous analyses. The dashed curves correspond to vanishing shape uncertainty. For these, as the exposure

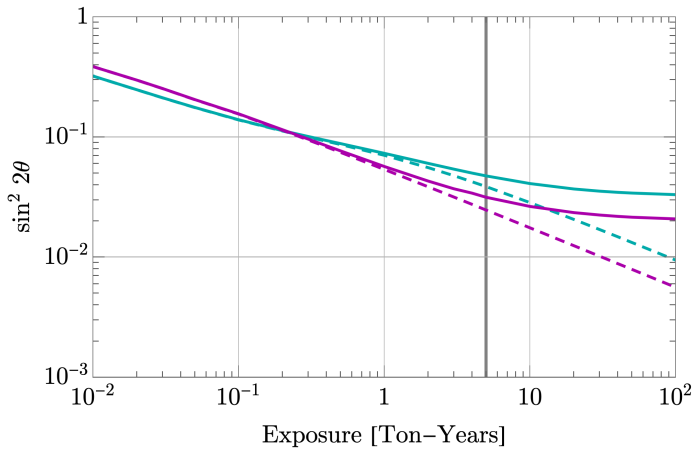

Figure 11: The sensitivity ($\Delta\chi^2 = 11.83$) to $\sin^2 2\theta$ as a function of exposure for a research reactor experiment with $L_{\text{near}} = 6$ m and $L_{\text{far}} = 9$ m. Cyan (magenta) curves correspond to $\Delta m^2 = 1$ eV^2 ($\Delta m^2 = 5$ eV^2). Dashed curves correspond to vanishing shape systematic uncertainty; solid curves take this to be 0.5%. The vertical, gray line indicates our benchmark 5 ton-years exposure.

is increased, the sensitivity improves without bound: the increase in statistics leads to an increasingly precise determination of the event rate at each position and in each energy bin, resulting in sensitivity that scales as $\sim$ (exposure)$^{-1/2}$. In contrast, the solid curves show the sensitivity including a 0.5% shape uncertainty. As the number of raw counts is increased, the fractional statistical uncertainty eventually becomes eclipsed by the shape uncertainty – the experiment becomes systematics limited. Past this point, the sensitivity saturates at some finite value. Inspection of Fig. 11 reveals that for our nominal 5 ton-year exposure, the experiment is already transitioning from being statistically limited to being systematically limited. Consequently, increasing the exposure beyond this value results in a negligible increase in sensitivity to $\sin^2 2\theta$.

6.3 Sterile Neutrino Sensitivity at TAO

The Taishan Antineutrino Observatory (TAO) is a future experiment whose main purpose is to produce a model-independent reference spectrum for the physics program at JUNO [84].

It is programmed to begging taking data in 2022 and is expected to achieve an unprecedented experimental resolution of the order $\sim 1.0\%/\sqrt{E[\mathrm{MeV}]}$. Though it is a *single-volume* detector, its fiducial volume may be *virtually* segmented, allowing for a multiple-baseline measurement of the sort outlined in the previous section. This segmentation is possible due to improvements in the coverage and efficiency of the photo sensors, as well as the precise timing resolution. This is a novel approach that has not been employed by existing searches for sterile neutrino. We have previously considered two detectors located at arbitrary baselines; here, on the other hand, we consider a fixed (core-to-detector) baseline position of 30 m and compare the spectra measured in each of its virtual segments. We will virtually segment the detector into either two or four equal-volume segments; the displacements between the barycenters and the center of the detector are ($\pm 3/8\ R$) and ($\pm\ 0.170\ R$, $\pm\ 0.580\ R$), respectively, $R = 0.65$ m being the radius of the fiducial volume at TAO. While virtual segmentation is an impressive capability of this detector, the fixed geometry is a nontrivial restriction on any multiple-baseline measurement.

We assume a total of 5 ton-year exposure from a 2.0 m radius core with an associated thermal power of 4.5 $\mathrm{GW_{th}}$, in broad agreement with the TAO conceptual design report (CDR) [11]. The fuel fractions of the core are assumed to be the same as our green-field studies Sec. 6.2. Moreover, a total of 60 bins between 2.0 to 8.0 MeV in prompt energy are considered. Background events are spread uniformly over the energy bins, assuming a total of 90 events per ton-day, consistent with those at NEOS [49]; we do not consider shape uncertainties on the background. Systematic uncertainties in this experiment are assumed to be consistent with those at STEREO [97]. Furthermore, a 0.5% bin-to-bin uncorrelated shape uncertainty is taken into account.

For our experimental configuration, we form the following χ^2 function:

$$\chi^2 = \sum_i^{N_{\mathrm{bin}}} \sum_j^{N_{\mathrm{seg}}} \left(\frac{M_{i,j} - \phi_i P_{i,j}\left(\sin^2 2\theta, \Delta m^2, \{\eta_\ell\}\right)}{\sigma_{i,j}} \right)^2 + \sum_\ell^{N_{\mathrm{sys}}} \left(\frac{\eta_\ell}{\sigma_\ell} \right)^2 . \tag{1}$$

This expression closely resembles Eq. 2, the salient difference being that we now index the N_{seg} ($= 2,\ 4$) segments with j. We account for the nonzero background and shape uncertainty in a similar fashion as Eq. 3 by defining $\sigma_{i,j}$ as

$$\sigma_{i,j} = \sqrt{P_{i,j}(1 + \sigma_{\mathrm{sh}}^2 \times P_{i,j}) + 2B_{i,j}}\ , \tag{2}$$

were $\sigma_{\rm sh}$ is the bin-to-bin shape uncertainty and $B_{i,j}$ is the (uniform) background in each energy bin i of segment j. The ϕ_i are flux nuisance parameters in each energy bin. As before, we analytically minimize the χ^2 with respect to these nuisance parameters to obtain

$$\phi_i = \frac{\sum_j \frac{M_{i,j} P_{i,j}}{(\sigma_{i,j})^2}}{\sum_j \left(\frac{P_{i,j}}{\sigma_{i,j}}\right)^2} \,, \tag{3}$$

where j runs over the detector segments. Lastly, the $\{\eta_\ell\}$ are the nuisance parameters describing our systematic uncertainties.

In Ref. [11], the Huber-Muller (HM) model [85, 57] is used to obtain the antineutrino energy spectrum with an introduction of a 5% bin-to-bin uncorrelated shape uncertainty. While we, too, use the HM fluxes, our analysis is not sensitive to this choice; by using the ϕ_i, our analysis employs a data-to-data spectral comparison, as compared to a data-to-model one. This removes any model dependence on our analysis, but reduces the number of degrees of freedom in the fit, leading to lower values of the χ^2 and, ultimately, less inferred statistical significance. Therefore, we expect the sensitivities obtained in this study to be less aggressive but more robust. Another important difference between our analysis and that of Ref. [11] is the assessment of the backgrounds: the collaboration publishes a combined rate of accidental, fast neutron and ^{9}Li/^{8}He decay backgrounds of ~ 450 events per ton-day, a more conservative figure than that assumed in our study. We have consciously elected to be more optimistic, given that the 90 events per ton-day we consider has been achieved at NEOS [49]. We also remind the reader that we only communicate sensitivities as contours of constant $\Delta\chi^2$, whereas Ref. [11] provides the results of Gaussian CL$_s$ analysis. This is not, strictly speaking, an apples-to-apples comparison of sensitivities; however, the gross features of the analyses are distinct enough that one can still draw important qualitative conclusions.

We show our results in Fig. 12. The dashed and solid cyan curves show the sensitivity ($\Delta\chi^2 = 11.83$) to sterile neutrinos for our analyses with two and four segments, respectively. The dot-dashed, magenta curve corresponds to the 99.7% CL$_s$ sensitivity from the TAO CDR [11]. We also show the 95% C.L. sensitivity from KATRIN in dashed gray, as well as the 3σ-preferred regions from Neutrino-4 [10] and from Ref. [9], in red and blue shading contours, respectively.

In the region $\Delta m^2 \leq 1$ eV^2, our analysis is substantially less sensitive than that of the CDR. This is a consequence of the (in)dependence on the flux model in these analyses. By

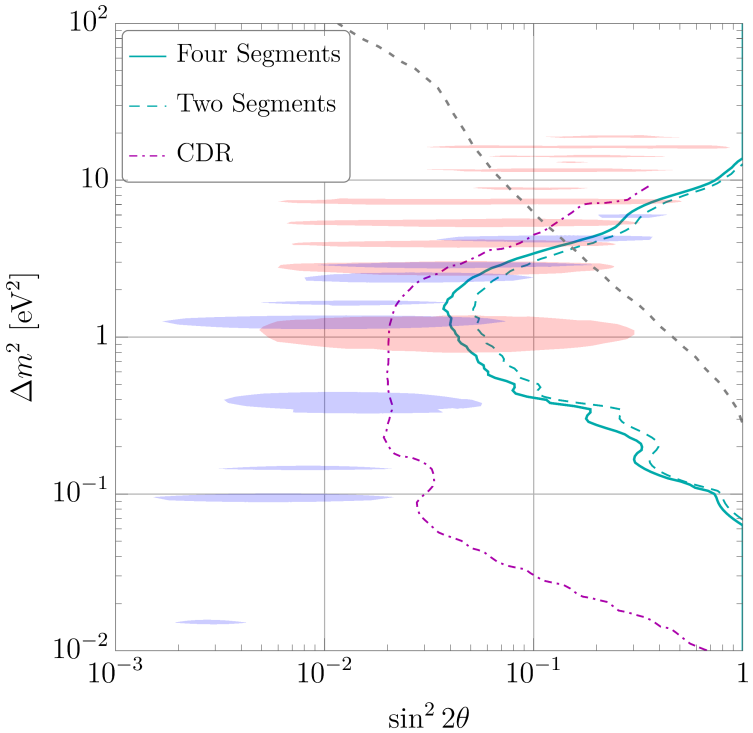

Figure 12: The sensitivity ($\Delta\chi^2 = 11.83$) to a sterile neutrino at TAO. Cyan curves correspond to our analysis with four (solid) or two (dashed) virtual segments. The dot-dashed, magenta curve corresponds to the 99.7% CL_s sensitivity presented in Ref. [11]. Also shown are the 95% C.L. sensitivity from KATRIN (dashed gray), as well as the 3σ-preferred regions from Neutrino-4 [10] (red shading) and from Ref. [9] (blue shading).

comparing directly to the HM flux model, the CDR analysis is sensitive to changes in the antineutrino spectrum induced over the ~ 30 m baseline between the core and the detector, affording sensitivity to lower values of Δm^2. In contrast, by comparing data to data, our analysis is sensitive only to changes induced over the ~ 1 m length scale spanned by the detector. Therefore, sensitivity to longer-wavelength oscillations is inevitably muted, and the barycenter of the sensitivity curve shifts to higher values of Δm^2. Furthermore, the addition of more segments improve the overall sensitivity; the gains, however, are modest. On one hand, increasing the number of segments increases the number of degrees of freedom

in the fit. On the other, this also increases the (statistical) uncertainty of the contents of any given energy bin. The former evidently outweighs the latter, though only marginally.

On balance, the sensitivity to sterile neutrinos presented in this study is less optimistic than the TAO CDR, but this is a consequence of having fundamentally different search strategies. Flux model independence is central to our analysis, as it was in the previous section. We believe this is conceptually more robust, though we have made some assumptions that are more optimistic than those presented in the CDR.

6.4 Lithium-8 doping of research reactors

As we have seen in the previous sections, the sensitivity to oscillations with $\Delta m^2 \gtrsim 2$ eV^2 is significantly improved if the near baseline is minimized as much as possible, due to (1) the increased event rate, and (2) high-frequency oscillations not averaging out. However, the physical layout of the facility severely constrains the possible location of a detector. Notice that because oscillations depend on the quantity $\Delta m^2 L/E$, the effect of reducing the baseline can be emulated by increasing the energies of the interacting antineutrinos. However, the energy spectrum of the antineutrinos emitted in fission is, of course, immutable.[17] In order to reach higher energies, then, one would need to consider a separate source of antineutrinos.

We consider precisely such a source, in the form of antineutrinos produced via the decays of ^{8}Li, produced by neutron capture on ^{7}Li. The main advantage is that the endpoint energy of these decays is ~ 13 MeV; this provides the high energies desired to extend the sensitivity of a sterile neutrino search to higher Δm^2. A similar proposal exists in the form of IsoDAR [94, 104], but implementing a ^{8}Li source at a nuclear reactor has the advantage that no new facilities are required to produce the neutrons that ultimately drive the source. If one can load the reactor core with enough ^{7}Li, then the excess neutrons produced in the core can, in principle, be used to generate these β decays.

In Fig. 13, we show the flux-weighted IBD cross section per ^{8}Li decay against the same per ^{235}U fission. Because the IBD cross section grows roughly quadratically in energy, the events associated with ^{8}Li β decay are disproportionately skewed to higher energies than those from fission. This results in a larger integrated flux-weighted cross section *per decay*; fewer antineutrinos are emitted per decay, but they are much more inclined to interact with the

[17] This is not strictly speaking true: the spectrum changes slightly as the composition of the reactor's fuel evolves. Here, we are referring to the impossibility of manipulating a given β decay into yielding more energetic neutrinos.

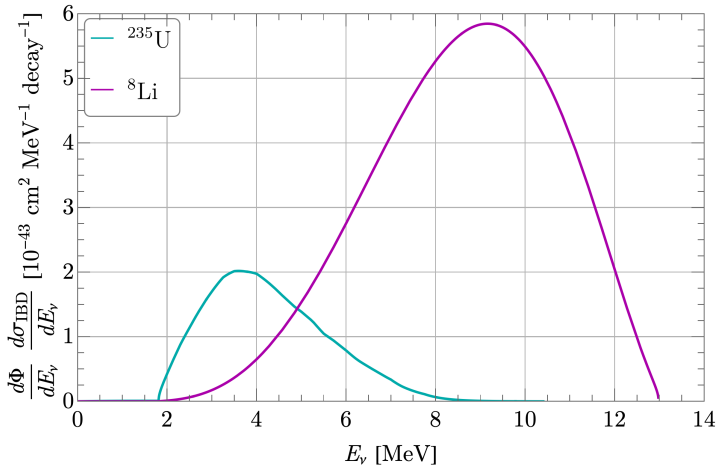

Figure 13: The flux-weighted cross section per decay for IBD detection of antineutrinos from ^{235}U fission (cyan) and from ^{8}Li β decay (magenta).

detector. However, while the per-decay rate of ^{8}Li events exceeds that of ^{235}U, it is unlikely that the absolute rate of ^{8}Li decay in an experiment could be arranged to be as large as the rate of ^{235}U fission. More broadly, there are a number of challenges in implementing ^{8}Li decays at nuclear reactors:

- Inserting ^{8}Li into a commercial core is essentially out of the question. This would require a significant interruption of operation of a core used to generate electricity and, consequently, income for the operator.

- Research reactor cores, in contrast, are constructed such that one may insert a sample of some material into the core to absorb some excess neutrons without disrupting the core. However, if one wanted to achieve lithium decay rates equal to the fission rate, then one would essentially need to absorb *every* excess neutron over the operation of the experiment. Apart from reactor physics constraints, this would monopolize the facility, that is, no neutrons would be available for any other user.

- Lastly, while natural lithium is dominantly ($\sim 92.4\%$) ^{7}Li, the thermal neutron capture cross section for ^{6}Li is roughly three orders of magnitude larger than that of ^{7}Li. Therefore, one would need high-purity ^{7}Li – around 99.9% – to ensure that the majority

of neutrons will ultimately produce ^{8}Li; to ensure that 90% of neutrons capture on ^{7}Li, this increases to nearly 99.99% purity. Scaling from previous results on Li-loading of HFIR [105] a 10% fraction of neutrinos may be possible in this case. Note, that high purity ^{7}Li is available in large quantities and considered as coolant in molten salt reactors.

In light of these restrictions, we expect that it may be possible to achieve a rate of one ^{8}Li decay for every five to ten fission events at a research core.

We employ a pseudoexperiment with $L_{\rm near} = 6$ m and $L_{\rm far} = 9$ m. The total exposure of the experiment is fixed to be 5 ton-years, apportioned between the two detectors according to their inverse-squared baseline, and we continue to assume that one year at a research reactor corresponds to three months of reactor-on time with an average power of 100 $\mathrm{MW_{th}}$. The rate of background events is still assumed to be 250 events per ton-day *in the region 2.0-8.0 MeV prompt energy*, i.e., 41.7 counts per ton-day per MeV; we assume that this rate extends out to 13 MeV. We further assume a TAO-like energy resolution and employ 100-keV bins between 2.0 and 12.0 MeV in prompt energy to take full advantage of this resolution. The systematics budget is the same as in previous studies and we ignore any bin-uncorrelated shape uncertainties.

The results are shown in Fig. 14. The cyan curve shows the sensitivity ($\Delta\chi^2 = 11.83$) in the absence of any added lithium, while the magenta curves introduce varying numbers of ^{8}Li decays per ^{235}U fission, which we denote $f_{^8\mathrm{Li}}$. The solid curve corresponds to $f_{^8\mathrm{Li}} = 1$, dashed to $f_{^8\mathrm{Li}} = 0.2$ and dotted to $f_{^8\mathrm{Li}} = 0.1$. We also show the projected sensitivity from KATRIN (dashed gray) and the 3σ-preferred regions from Neutrino-4 (red shading) and from Ref. [9] (blue shading). The benefit of including lithium decays is clear: for $f_{^8\mathrm{Li}} = 1$, the sensitivity improves by as much as an order of magnitude, particularly above $\Delta m^2 \gtrsim 5$ eV^2. In light of the aforementioned issues in the interpretation of the KATRIN constraint in the region $\Delta m^2 \lesssim 30$ eV^2, reactor experiments may be the only means by which to robustly probe a sterile neutrino in this region of parameter space — and a highly lithium-loaded reactor may even exceed the sensitivity of KATRIN above this value.

However, for reasons laid out above, there are a number of impediments to achieving $f_{^8\mathrm{Li}} = 1$. It would be more realistic to expect $f_{^8\mathrm{Li}}$ in the range $0.1 - 0.2$, in which case the dashed and dotted magenta lines should guide our interpretation of Fig. 14. The gains in sensitivity are more modest in this case. To compensate or this, one could envision increasing the exposure of the experiment. In Fig. 15a, left panel (a), we show how the sensitivity to oscillations with $\Delta m^2 = 1$ eV^2 evolves with the exposure; Fig. 15b, right panel (b), shows

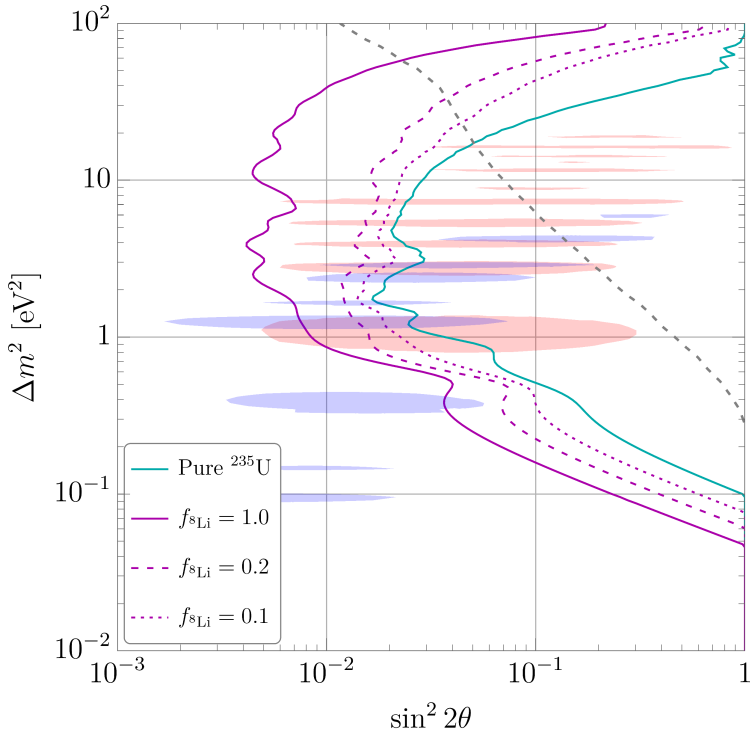

Figure 14: The sensitivity ($\Delta\chi^2 = 11.83$) of a lithium-loaded research reactor to a sterile neutrino. The sensitivity without ^{8}Li is shown in cyan while the magenta curves assume varying numbers of lithium decays per fission, $f_{^8\mathrm{Li}}$: 1.0 (solid), 0.2 (dashed) and 0.1 (dotted). We also show the 95% C.L. sensitivity from KATRIN (dashed gray), as well as the 3σ-preferred regions from Neutrino-4 [10] (red shading) and Ref. [9] (blue shading).

the same for $\Delta m^2 = 30$ eV^2. Cyan curves correspond to normal reactor conditions and magenta curves correspond to lithium loading with $f_{^8\mathrm{Li}} = 0.1$. Dashed curves corresponds to negligible shape systematics, whereas the solid curves introduce a 0.5% shape uncertainty.

From this figure, we see that our calculations with negligible shape uncertainty for a 5 ton-year exposure are in rough agreement with the sensitivities in the systematics-dominated limit. Moreover, the uranium-only and lithium-loaded curves asymptote to their ultimate sensitivities in lockstep. From the right panel (b) of Fig. 15b, in particular, it is clear that increasing the exposure for pure uranium does not recover the sensitivity to higher Δm^2

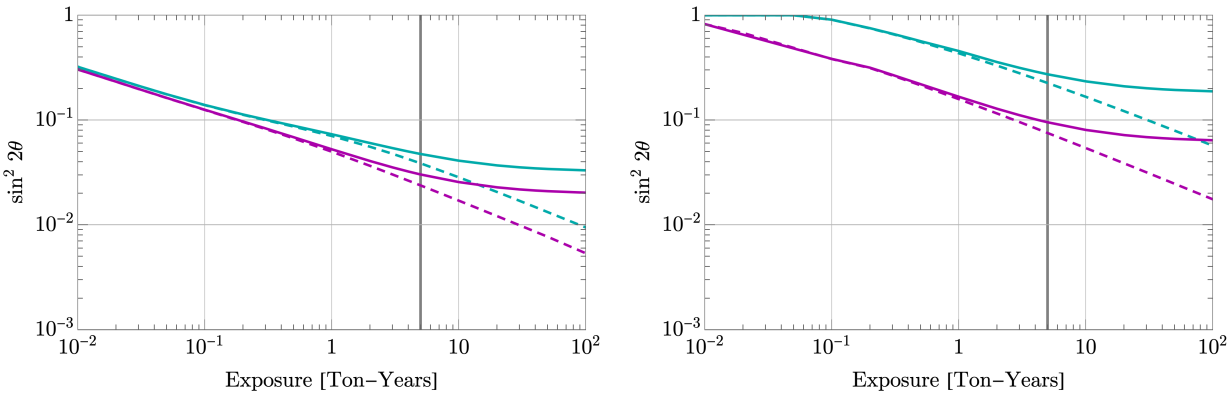

(a) (b)

Figure 15: The evolution of the sensitivity ($\Delta\chi^2 = 11.83$) to oscillations with $\Delta m^2 = 1$ eV^2 panel (a) and $\Delta m^2 = 30$ eV^2 panel (b) as a function of exposure for our lithium-enhanced research reactor pseudoexperiment. Cyan curves assume only ^{235}U is present and magenta curves introduce lithium with $f_{^8\mathrm{Li}} = 0.1$. Dashed curves ignore shape systematics and solid curves assume a 0.5% shape uncertainty. The vertical gray line indicates a 5 ton-year exposure.

obtained from adding even a small amount of lithium. Simply put, the increase in statistics between 2.0 and 8.0 MeV prompt energy is not enough to compensate for the total absence of events between 8.0 and 12.0 MeV. Given the choice between increasing the exposure of the experiment and increasing the lithium loading of the reactor, the latter is more effective in increasing the ultimate sensitivity.

In summary, our analysis suggests that loading a research core with highly enriched lithium is, from a physics perspective, an attractive possibility for enhancing the sensitivity of a reactor antineutrino experiment to a sterile neutrino, especially for moderately large values of Δm^2. That said, there are several practical hurdles that make any realization of such a concept technically demanding.

7 Conclusions

From our first work [65], we demonstrate the capabilities of tagged kaon beams in the disappearance channels of electron neutrinos and muon neutrinos to investigate intriguing indications from the Neutrino-4 and IceCube collaborations. The strength of the setup considered is the vanishingly small systematic errors from the beam flux and a virtually background free measurement. The drawback is the relatively low beam luminosity, as result of the need to tag kaon decays individually. The proposed setup is envisioned as add-on measurement to the cross section program of ENUBET. The physics case arises mainly from the Neutrino-4 result, which is in a Δm^2-region which ultimately may be hard for reactor neutrino experiments to test decisively. The proposed setup could decisively test either indication, IceCube at the $5\,\sigma$ level and Neutrino-4 at the $10\,\sigma$ level. This setup is not unique in this capability and of course dedicated facilities like nuSTORM [106] would provide superior sensitivity. In the hunt for the sterile neutrino, opportunistic measurements always have played a major role and we point out that if ENUBET is built and the Neutrino-4 indication persists, this setup would present such an opportunity.

From our second work [83], the green-field site optimization of short-baseline reactor experiments for their sensitivity to sterile neutrino oscillation, that is electron neutrino disappearance. The key to a sensitive experiment is the comparison of neutrino spectra measured at different baselines, which renders the results independent from reactor neutrino flux predictions. We perform the optimization by placing detectors at two baseline simultaneously and by finding the combination of baselines which provides the best overall sensitivity. In all cases studied, we find that two different baseline always perform much better than a single baseline experiment with double detector mass. We also find, that the baseline difference is of order meters and thus in principle can be accommodated within a single detector with position resolution, which we specifically illustrate with TAO. We look at two types of facilities: commercial reactors, with large cores, high power and a closest approach of 10-25 m; research reactors with compact cores, low power and a closest approach of 3-6 m. Experiments at commercial reactor clearly outperform research reactor for $\Delta m^2 < 1 - 2\,\mathrm{eV}^2$ under a variety of scenarios, whereas for larger $\Delta m^2 > 2\,\mathrm{eV}^2$ experiments at research reactors do better. For all cases, getting as close as possible with the best possible energy resolution is valuable. These results are summarized in Fig. 10.

We also investigate, how the sensitivity scales with exposure and find that is saturates at around 10 ton years even for systematics as small as 0.5%. We further extend the analysis by

looking at ^{7}Li doping of a reactor to create higher energy neutrinos: this results in enhanced sensitivity to large values of Δm^2 up $30\,\mathrm{eV}^2$ even for a modest, and potentially realistic, 10% lithium fraction.

Reactor neutrino experiments can offer a very good sensitivity to oscillations from $\Delta m^2 = 0.1 - 30\,\mathrm{eV}^2$ with ton-scale two-baseline experiments, where two or multiple baseline may be realized in the same detector. Sensitivities below $\sin^2 2\theta < 10^{-2}$ are possible even with reasonable systematics assumptions, pushing towards $\sin^2 2\theta < 10^{-3}$ however seems challenging. JUNO-TAO has very good sensitivity but does not compare to a purpose built experiment because of its relatively large distance to the reactor. Therefore, there is a strong case for a new dedicated commercial reactor experiment with good energy resolution, which currently does not exist. To cover the full range of mass squared splittings it is essential to use both research and commercial reactors.

8 References

References

[1] A. Aguilar-Arevalo et al. Evidence for neutrino oscillations from the observation of $\bar{\nu}_e$ appearance in a $\bar{\nu}_\mu$ beam. *Phys. Rev. D*, 64:112007, 2001.

[2] A.A. Aguilar-Arevalo et al. Significant Excess of ElectronLike Events in the MiniBooNE Short-Baseline Neutrino Experiment. *Phys. Rev. Lett.*, 121(22):221801, 2018.

[3] G. Mention, M. Fechner, Th. Lasserre, Th. A. Mueller, D. Lhuillier, M. Cribier, and A. Letourneau. Reactor antineutrino anomaly. *Phys. Rev. D*, 83:073006, Apr 2011.

[4] A.P. Serebrov et al. First Observation of the Oscillation Effect in the Neutrino-4 Experiment on the Search for the Sterile Neutrino. *Pisma Zh. Eksp. Teor. Fiz.*, 109(4):209–218, 2019.

[5] J. Kostensalo, J. Suhonen, C. Giunti, and P.C. Srivastava. The gallium anomaly revisited. *Physics Letters B*, 795:542–547, 2019.

[6] M. G. Aartsen et al. ev-scale sterile neutrino search using eight years of atmospheric muon neutrino data from the icecube neutrino observatory. *Phys. Rev. Lett.*, 125:141801, Sep 2020.

[7] M.G. Aartsen et al. Searching for ev-scale sterile neutrinos with eight years of atmospheric neutrinos at the icecube neutrino telescope. *Phys. Rev. D*, 102:052009, Sep 2020.

[8] P. Adamson et al. Improved constraints on sterile neutrino mixing from disappearance searches in the minos, MINOS+, daya bay, and bugey-3 experiments. *Phys. Rev. Lett.*, 125:071801, Aug 2020.

[9] Jeffrey M. Berryman and Patrick Huber. Sterile Neutrinos and the Global Reactor Antineutrino Dataset. *JHEP*, 01:167, 2021.

[10] A. P. Serebrov. Present status of Neutrino-4 experiment search for sterile neutrino.

[11] Angel Abusleme et al. TAO Conceptual Design Report: A Precision Measurement of the Reactor Antineutrino Spectrum with Sub-percent Energy Resolution. 5 2020.

[12] P. F. de Salas, D. V. Forero, S. Gariazzo, P. Martínez-Miravé, O. Mena, C. A. Ternes, M. Tórtola, and J. W. F. Valle. 2020 global reassessment of the neutrino oscillation picture. *JHEP*, 02:071, 2021.

[13] J. Chadwick. Possible Existence of a Neutron. *Nature*, 129:312, 1932.

[14] G. W. Rodeback and J. S. Allen. Neutrino recoils following the capture of orbital electrons in A-37. *Camb. Monogr. Part. Phys. Nucl. Phys. Cosmol.*, 14:28–37, 2000.

[15] Frederick Reines and Clyde L. Cowan. The neutrino. *Nature*, 178:446–449, 1956.

[16] J. J. Thomson. Cathode rays. *Phil. Mag. Ser. 5*, 44:293–316, 1897.

[17] E. Fermi. An attempt of a theory of beta radiation. 1. *Z. Phys.*, 88:161–177, 1934.

[18] R. P. Feynman and M. Gell-Mann. Theory of the fermi interaction. *Phys. Rev.*, 109:193–198, Jan 1958.

[19] S. L. Glashow. Partial Symmetries of Weak Interactions. *Nucl. Phys.*, 22:579–588, 1961.

[20] Steven Weinberg. A Model of Leptons. *Phys. Rev. Lett.*, 19:1264–1266, 1967.

[21] Abdus Salam. Weak and Electromagnetic Interactions. *Conf. Proc. C*, 680519:367–377, 1968.

[22] G. Arnison et al. Experimental Observation of Events with Large Missing Transverse Energy Accompanied by a Jet Or a Photon(s) in p anti-p Collisions at s**(1/2)=540-GeV. *Phys. Lett. B*, 139:115, 1984.

[23] M. Banner et al. Observation of Single Isolated Electrons of High Transverse Momentum in Events with Missing Transverse Energy at the CERN anti-p p Collider. *Phys. Lett. B*, 122:476–485, 1983.

[24] T. D. Lee and C. N. Yang. Question of parity conservation in weak interactions. *Phys. Rev.*, 104:254–258, Oct 1956.

[25] C. S. Wu, E. Ambler, R. W. Hayward, D. D. Hoppes, and R. P. Hudson. Experimental test of parity conservation in beta decay. *Phys. Rev.*, 105:1413–1415, Feb 1957.

[26] G. Danby, J-M. Gaillard, K. Goulianos, L. M. Lederman, N. Mistry, M. Schwartz, and J. Steinberger. Observation of high-energy neutrino reactions and the existence of two kinds of neutrinos. *Phys. Rev. Lett.*, 9:36–44, Jul 1962.

[27] K. Kodama et al. Observation of tau neutrino interactions. *Phys. Lett. B*, 504:218–224, 2001.

[28] B. Pontecorvo. Mesonium and anti-mesonium. *Sov. Phys. JETP*, 6:429, 1957.

[29] Ziro Maki, Masami Nakagawa, and Shoichi Sakata. Remarks on the unified model of elementary particles. *Prog. Theor. Phys.*, 28:870–880, 1962.

[30] Y. Fukuda et al. Evidence for oscillation of atmospheric neutrinos. *Phys. Rev. Lett.*, 81:1562–1567, Aug 1998.

[31] Q. R. Ahmad et al. Direct evidence for neutrino flavor transformation from neutral-current interactions in the sudbury neutrino observatory. *Phys. Rev. Lett.*, 89:011301, Jun 2002.

[32] P.A. Zyla et al. Review of Particle Physics. *PTEP*, 2020(8):083C01, 2020.

[33] K. Abe et al. Search for *cp* violation in neutrino and antineutrino oscillations by the t2k experiment with 2.2×10^{21} protons on target. *Phys. Rev. Lett.*, 121:171802, Oct 2018.

[34] M. A. Acero et al. New constraints on oscillation parameters from ν_e appearance and ν_μ disappearance in the nova experiment. *Phys. Rev. D*, 98:032012, Aug 2018.

[35] S. P. Mikheev and A. Yu. Smirnov. Resonant amplification of neutrino oscillations in matter and solar neutrino spectroscopy. *Nuovo Cim. C*, 9:17–26, 1986.

[36] L. Wolfenstein. Neutrino oscillations in matter. *Phys. Rev. D*, 17:2369–2374, May 1978.

[37] K. Eguchi et al. First results from KamLAND: Evidence for reactor anti-neutrino disappearance. *Phys. Rev. Lett.*, 90:021802, 2003.

[38] John N. Bahcall. Solar neutrinos. i. theoretical. *Phys. Rev. Lett.*, 12:300–302, Mar 1964.

[39] Y. Abe et al. Indication of Reactor $\bar{\nu}_e$ Disappearance in the Double Chooz Experiment. *Phys. Rev. Lett.*, 108:131801, 2012.

[40] F. P. An et al. Observation of electron-antineutrino disappearance at Daya Bay. *Phys. Rev. Lett.*, 108:171803, 2012.

[41] J. K. Ahn et al. Observation of reactor electron antineutrinos disappearance in the reno experiment. *Phys. Rev. Lett.*, 108:191802, May 2012.

[42] M. A. Acero et al. First measurement of neutrino oscillation parameters using neutrinos and antineutrinos by nova. *Phys. Rev. Lett.*, 123:151803, Oct 2019.

[43] K. Abe et al. Constraint on the matter–antimatter symmetry-violating phase in neutrino oscillations. *Nature*, 580(7803):339–344, 2020. [Erratum: Nature 583, E16 (2020)].

[44] Ivan Esteban, M. C. Gonzalez-Garcia, Michele Maltoni, Thomas Schwetz, and Albert Zhou. The fate of hints: updated global analysis of three-flavor neutrino oscillations. *JHEP*, 09:178, 2020.

[45] Peter W. Higgs. Broken symmetries and the masses of gauge bosons. *Phys. Rev. Lett.*, 13:508–509, Oct 1964.

[46] F. Englert and R. Brout. Broken symmetry and the mass of gauge vector mesons. *Phys. Rev. Lett.*, 13:321–323, Aug 1964.

[47] Georges Aad et al. Observation of a new particle in the search for the Standard Model Higgs boson with the ATLAS detector at the LHC. *Phys. Lett. B*, 716:1–29, 2012.

[48] Serguei Chatrchyan et al. Observation of a New Boson at a Mass of 125 GeV with the CMS Experiment at the LHC. *Phys. Lett. B*, 716:30–61, 2012.

[49] Y. J. Ko et al. Sterile neutrino search at the neos experiment. *Phys. Rev. Lett.*, 118:121802, Mar 2017.

[50] I Alekseev et al. Search for sterile neutrinos at the DANSS experiment. *Phys. Lett. B*, 787:56–63, 2018.

[51] Mona Dentler, Álvaro Hernández-Cabezudo, Joachim Kopp, Pedro A. N. Machado, Michele Maltoni, Ivan Martinez-Soler, and Thomas Schwetz. Updated Global Analysis of Neutrino Oscillations in the Presence of eV-Scale Sterile Neutrinos. *JHEP*, 08:010, 2018.

[52] J. M. Conrad and M. H. Shaevitz. Sterile Neutrinos: An Introduction to Experiments. *Adv. Ser. Direct. High Energy Phys.*, 28:391–442, 2018.

[53] A. A. Aguilar-Arevalo et al. The MiniBooNE Detector. *Nucl. Instrum. Meth. A*, 599:28–46, 2009.

[54] B. Armbruster et al. Upper limits for neutrino oscillations $\overline{\nu}_\mu \to \overline{\nu}_e$ from muon decay at rest. *Phys. Rev. D*, 65:112001, Jun 2002.

[55] M Antonello et al. Experimental search for the "LSND anomaly" with the ICARUS detector in the CNGS neutrino beam. *Eur. Phys. J. C*, 73(3):2345, 2013.

[56] P. Astier et al. Search for nu(mu) —> nu(e) oscillations in the NOMAD experiment. *Phys. Lett. B*, 570:19–31, 2003.

[57] Patrick Huber. On the determination of anti-neutrino spectra from nuclear reactors. *Phys. Rev.*, C84:024617, 2011. [Erratum: Phys. Rev. C85, 029901 (2012)].

[58] J. N. Abdurashitov et al. Measurement of the solar neutrino capture rate with gallium metal. iii. results for the 2002–2007 data-taking period. *Phys. Rev. C*, 80:015807, Jul 2009.

[59] W. Hampel et al. GALLEX solar neutrino observations: Results for GALLEX IV. *Phys. Lett. B*, 447:127–133, 1999.

[60] Jeffrey M. Berryman. Constraining Sterile Neutrino Cosmology with Terrestrial Oscillation Experiments. *Phys. Rev.*, D100(2):023540, 2019.

[61] S. Gariazzo, P. F. de Salas, and S. Pastor. Thermalisation of sterile neutrinos in the early Universe in the 3+1 scheme with full mixing matrix. *JCAP*, 07:014, 2019.

[62] Steffen Hagstotz, Pablo F. de Salas, Stefano Gariazzo, Martina Gerbino, Massimiliano Lattanzi, Sunny Vagnozzi, Katherine Freese, and Sergio Pastor. Bounds on light sterile neutrino mass and mixing from cosmology and laboratory searches. 3 2020.

[63] Matthew Adams, Fedor Bezrukov, Jack Elvin-Poole, Justin J. Evans, Pawel Guzowski, Brían Ó. Fearraigh, and Stefan Söldner-Rembold. Direct comparison of sterile neutrino constraints from cosmological data, ν_e disappearance data and $\nu_\mu \to \nu_e$ appearance data in a $3+1$ model. *Eur. Phys. J. C*, 80(8):758, 2020.

[64] M. Aker et al. Improved Upper Limit on the Neutrino Mass from a Direct Kinematic Method by KATRIN. *Phys. Rev. Lett.*, 123(22):221802, 2019.

[65] Luis Delgadillo and Patrick Huber. Sterile neutrino searches at tagged kaon beams. *Phys. Rev. D*, 103(3):035018, 2021.

[66] A. Longhin, L. Ludovici, and F. Terranova. A novel technique for the measurement of the electron neutrino cross section. *Eur. Phys. J. C*, 75(4):155, 2015.

[67] F. Acerbi et al. A high precision neutrino beam for a new generation of short baseline experiments. 1 2019.

[68] F. Pupilli. private communication, 2020.

[69] Patrick Huber, M. Lindner, and W. Winter. Simulation of long-baseline neutrino oscillation experiments with GLoBES (General Long Baseline Experiment Simulator). *Comput. Phys. Commun.*, 167:195, 2005.

[70] Patrick Huber, Joachim Kopp, Manfred Lindner, Mark Rolinec, and Walter Winter. New features in the simulation of neutrino oscillation experiments with GLoBES 3.0: General Long Baseline Experiment Simulator. *Comput. Phys. Commun.*, 177:432–438, 2007.

[71] Joachim Kopp. Efficient numerical diagonalization of hermitian 3 x 3 matrices. *Int. J. Mod. Phys. C*, 19:523–548, 2008.

[72] Joachim Kopp, Manfred Lindner, Toshihiko Ota, and Joe Sato. Impact of non-standard neutrino interactions on future oscillation experiments. In *15th International Conference on Supersymmetry and the Unification of Fundamental Interactions (SUSY07)*, pages 756–759, 10 2007.

[73] P. Adamson et al. Measurement of single π^0 production by coherent neutral-current ν Fe interactions in the MINOS Near Detector. *Phys. Rev. D*, 94(7):072006, 2016.

[74] M.A. Acero et al. Measurement of neutrino-induced neutral-current coherent π^0 production in the NOvA near detector. *Phys. Rev. D*, 102(1):012004, 2020.

[75] Ch. Berger and L. M. Sehgal. Partially conserved axial vector current and coherent pion production by low energy neutrinos. *Phys. Rev. D*, 79:053003, Mar 2009.

[76] A. Longhin. Novel neutrino beams. talk presented at Neutrino 2020 conference, 2020.

[77] A.P. Serebrov et al. Preparation of the Neutrino-4 experiment on search for sterile neutrino and the obtained results of measurements. 5 2020.

[78] Pilar Coloma, Patrick Huber, and Thomas Schwetz. Statistical interpretation of sterile neutrino oscillation searches at reactors. 8 2020.

[79] S. Axani, G. Collin, J. M. Conrad, M. H. Shaevitz, J. Spitz, and T. Wongjirad. Decisive disappearance search at high Δm^2 with monoenergetic muon neutrinos. *Phys. Rev. D*, 92:092010, Nov 2015.

[80] M. Apollonio et al. Search for neutrino oscillations on a long baseline at the CHOOZ nuclear power station. *Eur. Phys. J. C*, 27:331–374, 2003.

[81] F. Boehm et al. Final results from the Palo Verde neutrino oscillation experiment. *Phys. Rev. D*, 64:112001, 2001.

[82] C. Giunti. Statistical Significance of Reactor Antineutrino Active-Sterile Oscillations. 4 2020.

[83] Jeffrey M. Berryman, Luis A. Delgadillo, and Patrick Huber. Future Searches for Light Sterile Neutrinos at Nuclear Reactors. 3 2021.

[84] Fengpeng An et al. Neutrino Physics with JUNO. *J. Phys. G*, 43(3):030401, 2016.

[85] Th. A. Mueller et al. Improved Predictions of Reactor Antineutrino Spectra. *Phys. Rev.*, C83:054615, 2011.

[86] K. N. Abazajian et al. Light Sterile Neutrinos: A White Paper. 2012.

[87] Sebastian Böser, Christian Buck, Carlo Giunti, Julien Lesgourgues, Livia Ludhova, Susanne Mertens, Anne Schukraft, and Michael Wurm. Status of Light Sterile Neutrino Searches. 2019.

[88] Jeffrey M. Berryman and Patrick Huber. Reevaluating Reactor Antineutrino Anomalies with Updated Flux Predictions. *Phys. Rev. D*, 101(1):015008, 2020.

[89] V. Kopeikin, M. Skorokhvatov, and O. Titov. Reevaluating reactor antineutrino spectra with new measurements of the ratio between ^{235}U and ^{239}Pu β spectra. 3 2021.

[90] Jeffrey M. Berryman, Vedran Brdar, and Patrick Huber. Particle physics origin of the 5 MeV bump in the reactor antineutrino spectrum? *Phys. Rev.*, D99(5):055045, 2019.

[91] Christian Grieb, Jonathan Link, and R. S. Raghavan. Probing active to sterile neutrino oscillations in the LENS detector. *Phys. Rev. D*, 75:093006, 2007.

[92] G. Bellini et al. SOX: Short distance neutrino Oscillations with BoreXino. *JHEP*, 08:038, 2013.

[93] Sanjib K. Agarwalla, Patrick Huber, and Jonathan M. Link. Constraining sterile neutrinos with a low energy beta-beam. *JHEP*, 01:071, 2010.

[94] J. M. Conrad, M. H. Shaevitz, I. Shimizu, J. Spitz, M. Toups, and L. Winslow. Precision $\bar{\nu}_e$-electron scattering measurements with IsoDAR to search for new physics. *Phys. Rev. D*, 89(7):072010, 2014.

[95] D. Adey et al. Light sterile neutrino sensitivity at the nuSTORM facility. *Phys. Rev. D*, 89(7):071301, 2014.

[96] M. Andriamirado et al. Improved short-baseline neutrino oscillation search and energy spectrum measurement with the PROSPECT experiment at HFIR. *Phys. Rev. D*, 103(3):032001, 2021.

[97] H. Almazán et al. Improved sterile neutrino constraints from the stereo experiment with 179 days of reactor-on data. *Phys. Rev. D*, 102:052002, Sep 2020.

[98] Matteo Agostini and Birgit Neumair. Statistical Methods for the Search of Sterile Neutrinos. 2019.

[99] X. Qian, A. Tan, J. J. Ling, Y. Nakajima, and C. Zhang. The Gaussian CL_s method for searches of new physics. *Nucl. Instrum. Meth. A*, 827:63–78, 2016.

[100] Gary J. Feldman and Robert D. Cousins. A Unified approach to the classical statistical analysis of small signals. *Phys. Rev.*, D57:3873–3889, 1998.

[101] G. Agnolet et al. Background Studies for the MINER Coherent Neutrino Scattering Reactor Experiment. *Nucl. Instrum. Meth.*, A853:53–60, 2017.

[102] Mikhail Danilov. Recent results of the DANSS experiment. In *2019 European Physical Society Conference on High Energy Physics*, 11 2019.

[103] M. Aker et al. Bound on 3+1 active-sterile neutrino mixing from the first four-week science run of KATRIN. 11 2020.

[104] Jose R. Alonso and K. Nakamura. IsoDAR@KamLAND: A Conceptual Design Report for the Conventional Facilities. 2017.

[105] Andrew Conant. *ANTINEUTRINO SPECTRUM CHARACTERIZATION OF THE HIGH FLUX ISOTOPE REACTOR USING NEUTRONIC SIMULATIONS*. PhD thesis, Georgia Tech, 2018.

[106] D. Adey et al. Light sterile neutrino sensitivity at the nustorm facility. *Phys. Rev. D*, 89:071301, Apr 2014.

[heading=none]

A Appendix

A.1 Averaging Oscillations Over Production Region

If the geometry of an experiment is such that the extent of the core or detector (or both) is not small compared to the distance between them, or if the wavelength associated with a particular oscillation is smaller than either of these, then the expression for the oscillation probability in Eq. (1) must be flux-averaged over the production and detection regions. In this case, the proper oscillation probability is formally given by

$$\langle P_{\overline{ee}} \rangle = \frac{\int d^3\vec{x}\, d^3\vec{y}\, \dfrac{P_{\overline{ee}}}{|\vec{y}-\vec{x}|^2}}{\int d^3\vec{x}\, d^3\vec{y}\, \dfrac{1}{|\vec{y}-\vec{x}|^2}}, \tag{1}$$

where $\vec{x}$ and $\vec{y}$ are the integration variables over the volumes of the core and detector, respectively, and the factor of $\frac{1}{|\vec{y}-\vec{x}|^2}$ in either integral accounts for the inverse-square dependence of the flux. For the pseudoexperiments we consider, the detector is assumed point-like; the integral over $d^3\vec{y}$ results in a trivial replacement $\vec{y} \to \vec{L}$, the displacement between the center of the core and the detector. Moreover, we approximate the core to be a sphere of radius R. Therefore, we may rewrite Eq. (1) as

$$\langle P_{\overline{ee}} \rangle = 1 - \sin^2 2\theta \times \frac{\displaystyle\int \frac{dr\, d\cos\phi\; r^2 \sin^2\left(q\sqrt{L^2+r^2+2rL\cos\phi}\right)}{L^2+r^2+2rL\cos\phi}}{\displaystyle\int \frac{dr\, d\cos\phi\; r^2}{L^2+r^2+2rL\cos\phi}} \equiv 1 - \sin^2 2\theta \times F(q), \tag{2}$$

where we have employed Eq. (1) and abbreviated $q \equiv \frac{\Delta m^2}{4E_\nu}$. The function $F(q)$ may be evaluated analytically:

$$\begin{aligned} F(q) = \frac{1}{2} + \Big\{ & 4qR\sin(2qL)\cos(2qR) - 4qL\sin(2qR)\cos(2qL) - 2\sin(2qL)\sin(2qR) \\ & + 4q^2(L^2-R^2)\Big[\mathrm{Ci}\big(2q(L+R)\big) - \mathrm{Ci}\big(2q(L-R)\big)\Big]\Big\} \times \qquad (3) \\ & \Big\{16q^2RL - 8q^2(L^2-R^2)\ln\left(\frac{L+R}{L-R}\right)\Big\}^{-1}, \qquad (4) \end{aligned}$$

where $\mathrm{Ci}(x)$ is the cosine integral function, defined as

$$\mathrm{Ci}(x) = -\int_x^\infty dt\, \frac{\cos(t)}{t}. \tag{5}$$

One can verify from Eq. (4) that $F(q) \to \sin^2(qL)$ as $R \to 0$.